

# PAN2 maintains mRNA poly(A) tail homeostasis and regulates translation during spermiogenesis in mice

Received: 29 July 2025

Accepted: 6 February 2026

Published online: 19 February 2026

 Check for updatesXuan Wu<sup>1</sup>, Yu-Ke Wu<sup>1</sup>, Meng-Yan Jia<sup>1</sup>, Zhuoyue Niu<sup>2,3</sup>, Jingwen Liu<sup>2,3</sup>, Wen-Jing Wang<sup>1</sup>, Zhi-Yan Jiang<sup>1</sup>, Falong Lu<sup>2,3</sup>  , Lu Chen<sup>4</sup>  , Liling Liu<sup>5</sup>   & Heng-Yu Fan<sup>1</sup>  

The elongation and shortening of poly(A) tails are the most common types of post-transcriptional mRNA regulation in eukaryotic cells. PAN2-PAN3 and CCR4-NOT complexes are the main cytoplasmic enzymes that trim the poly(A) tails of mRNAs. However, the *in vivo* function of PAN2-PAN3 in mammals remains unclear. Here, we found that the germline-specific deletion of *Pan2* causes male infertility due to a step-8/9 spermatogenic arrest, while meiotic prophase proceeds normally. Using PAI-seq2 and mass spectrometry analyses, we define stage-specific remodeling of poly(A) tails that is disrupted in *Pan2*-null round spermatids (RS). Ribo-lite reveals a global reduction in translation efficiency in *Pan2*-deficient RS, correlating with proteomic changes and impairing pathways for spermatid differentiation. Endogenous IP-MS identifies PAN2 association with PABPC1 and initiation factors (EIF4E, EIF4A1, EIF5A), whose protein levels decline upon *Pan2* loss, indicating compromised stability of key translational machinery. Together, these findings highlight the important physiological functions of PAN2 in spermiogenesis and expand our understanding of the post-transcriptional regulation of mRNAs in specific physiological processes.

In the cytoplasm, mRNA is regulated at both its 5' and 3' ends to facilitate the translation of proteins essential for the organism's life activities<sup>1</sup>. Erroneous or unnecessary mRNAs are degraded by exonucleases and their cofactors. The degradation process begins with the shortening of the 3' poly(A) tail. The PAN2-PAN3 complex and the CCR4-NOT complex work synergistically to promote the cascade of deadenylation at the 3' poly(A) tail of mRNA in eukaryotes, aiding in its degradation<sup>2</sup>. Immediately after polyadenylation, the average length of mammalian poly(A) tails ranges from 150 to 250 nt<sup>3</sup>. However, the dynamic nature of poly(A) tails becomes apparent in the cytoplasm,

and their steady-state length stabilizes at approximately 80–110 nt in mammals, reflecting a finely regulated balance between degradation and elongation<sup>4</sup>. The PAN2-PAN3 complex initiates deadenylation and shortens the unstable poly(A) tails of mRNA. Poly(A) specific ribonuclease subunit 2 (PAN2) serves as the catalytic subunit of this complex. PAN2 binds to the poly(A) tail of the target mRNA via the linker protein PAN3 to perform deadenylation. PAN3 can attach to the poly(A) tail of mRNA through its PAM2 domain and interact with the C-terminus of the poly(A) binding protein (PABP) to associate with the mRNA. Together, one PAN2 and two PAN3 subunits form a stable complex that

<sup>1</sup>Life Sciences Institute, Zhejiang Key Laboratory of Precise Protection and Promotion of Fertility, Assisted Reproduction Unit, Department of Obstetrics and Gynecology, Sir Run Run Shaw Hospital, Zhejiang University, Hangzhou, China. <sup>2</sup>Laboratory of Integrative Physiology, Institute of Genetics and Developmental Biology, Chinese Academy of Sciences, Beijing, China. <sup>3</sup>University of Chinese Academy of Sciences, Beijing, China. <sup>4</sup>State Key Laboratory of Female Fertility Promotion, Center for Reproductive Medicine, Department of Obstetrics and Gynecology, Peking University Third Hospital, Beijing, China. <sup>5</sup>Department of Reproductive Medicine and Genetics Center, The People's Hospital of Guangxi Zhuang Autonomous Region, Nanning, Guangxi, China.

 e-mail: [fillu@genetics.ac.cn](mailto:fillu@genetics.ac.cn); [L\\_chen@hsc.pku.edu.cn](mailto:L_chen@hsc.pku.edu.cn); [liulilingnn@126.com](mailto:liulilingnn@126.com); [hyfan@zju.edu.cn](mailto:hyfan@zju.edu.cn)

carries out deadenylation, while PABP enhances the activity of the PAN2-PAN3 complex<sup>5</sup>. When the polyA tail of the mRNA is reduced to less than 110–150 nucleotides, the catalytic activity of the PAN2-PAN3 complex is inhibited, allowing the CCR4-NOT complex to take over and facilitate deadenylation<sup>2,6</sup>.

Various degradation-related enzymes play crucial roles in spermatogenesis. Some subunits of the CCR4-NOT complex have been reported to be closely related to spermatogenesis. *Cnot4* knockout in male mouse germ cells affects XY chromosome pairing and induces double-strand break repair abnormalities, leading to the arrest of spermatogenesis in pachytene/diplotene spermatocytes<sup>7</sup>. Knockout of *Cnot7*, the catalytic subunit of the CCR4-NOT complex, significantly reduces sperm quality and leads to male infertility in mice<sup>8,9</sup>. However, not all subunits of the CCR4-NOT complex affect male reproduction. For example, CNOT6L is essential for female fertility, but has no significant effect on male reproduction<sup>10</sup>. Terminal uridylyltransferase 4/7 (TUT4/7), which are downstream of CCR4-NOT, are the major cellular terminal uridylyltransferases that mediate the uridylation of miRNA and mRNA. Their uridylation is required for the clearance of expressed transcripts when pachytene spermatocytes reach the diplotene stage during meiosis<sup>11</sup>. Furthermore, the loss of DIS3-like 3'–5' exonuclease 2 (DIS3L2) downstream of TUT4/7 in spermatocytes leads to defective spermatogenesis and male infertility<sup>12</sup>. Deletion of the PAN2-PAN3 complex upstream of CCR4-NOT in human cells specifically increases tail length by more than 150 nt, but this altered mRNA represents only a small fraction of the total mRNA. Similarly, deleting the genes encoding *Pan2* or *Pan3* in yeast leads to longer poly(A) tails, but does not eliminate deadenylation<sup>2,13</sup>. Whether PAN2, as a member of the complex that initiates deadenylation, regulates the poly(A) tail of mRNA during spermatogenesis, and whether it has important physiological functions have not been elucidated.

Poly(A) tails contribute to the translational status and stability of mRNAs and thus, function as master regulators of gene expression in the cytoplasm<sup>14,15</sup>. In many cases, the poly(A) tail is the first checkpoint that protects mRNA. Deadenylation typically occurs before decapping, placing the poly(A) tail at a critical point in mRNA decay. The traditional view is that the length of poly(A) tail positively correlates with translation efficiency<sup>16,17</sup>. However, previous studies have shown that mRNAs with higher translation rates, such as those of ribosomal and other housekeeping genes, have short poly(A) tail lengths, mostly 30 or 60 nucleotides<sup>17,18</sup>. In the cytoplasm, the poly(A) tail is bound to PABPC<sup>16</sup>. PABPC requires approximately 12 adenosine molecules for high-affinity binding, but physically covers approximately 30 nucleotides. For example, longer poly(A) tails bind more PABPC<sup>16</sup>. PABPC1 is also closely related to the regulation of poly(A) tail length and the translation process<sup>19</sup>. In addition, PABPC and the 5' end of eukaryotic translation initiation factor 4E (EIF4E) and eukaryotic translation initiation factor 4G (EIF4G) build a “closed loop”<sup>20</sup>, and PABPC also stimulates another translation initiation factor, EIF4A, by enhancing its ATPase and helicase activities<sup>21</sup>. Therefore, mRNA can form the “closed loop” that links communication between the 5' cap and the 3' poly(A) tail<sup>22</sup>.

The process by which diploid spermatogonial stem cells in male mammals generate haploid sperm is called spermatogenesis, including mitosis, meiosis, and spermiogenesis<sup>23</sup>. Spermiogenesis is strictly regulated and is divided into 16 stages. Haploid sperm undergo a series of complex structural changes, including acrosome formation, chromatin remodeling, nuclear compaction, and sperm tail formation<sup>24</sup>. In addition, haploid male germ cells display uncoupled transcription and translation<sup>25–27</sup>. Once the round spermatids (RS) begin to elongate, transcription is turned off because of the onset of nuclear condensation<sup>26,28</sup>. However, many key transcripts are required for translation during sperm cell elongation, differentiation, and assembly into mature sperm. Thus, translational regulation is critical for spermatogenesis<sup>29</sup>. The relationship between the poly(A) tail and

translation during spermiogenesis has not been fully elucidated, and an exploration of PAN2 function during spermiogenesis will help us better explore this issue.

Previous studies have shown that cytoplasmic poly(A) polymerase, deadenylation enzymes, and poly(A)-binding proteins are essential for spermatogenesis. For example, several studies have used the Oxford Nanopore Direct RNA Sequencing (DRS) method to comprehensively analyze poly(A) tails in mouse testes and ovaries<sup>30</sup>. They report that the polyadenylation of mRNA encoding secreted proteins, mediated by TENT5, is essential for mouse gametogenesis<sup>31</sup>. But the regulation of mRNA tail length has not been fully elucidated because of the limitations of sequencing technology<sup>27,32,33</sup>. With the development of third-generation sequencing, the technology for determining the poly(A) tail length and its components has become increasingly mature, which overcomes problems such as sensitivity and low input volume and provides an effective method to explore the effect of poly(A) tail length on spermatogenesis<sup>34,35</sup>. The PALso-seq2 technique used in this study can analyze both the length and sequence of poly(A) tails<sup>36</sup>. As a model for the uncoupling of transcription and translation, sperm also allows us to better understand the role of poly(A) tail length and related proteins in the regulation of translation<sup>29</sup>.

In this study, we demonstrated that PAN2 plays an indispensable role in spermiogenesis and is essential for maintaining the stability of the mRNA poly(A) tail length and translation regulation during this stage, providing a new perspective on the relationship between the poly(A) tail and translation regulation.

## Results

### PAN2 is essential for mouse spermatogenesis and male fertility

Regulation of the mRNA poly(A) tail is closely related to mRNA deadenylation. PAN2 is considered to be the main catalytic enzyme that regulates the initiation of deadenylation; however, its physiological role in sperm development remains unknown. We first evaluated whether the expression of deadenylase PAN2 was organ- or cell-specific. The RT-qPCR results showed that the mRNA expression level of *Pan2* in the testes was very high, and the western blotting results showed that the PAN2 protein was enriched in adult mouse testes and ovaries (Fig. 1a, b). Since the commercially available anti-PAN2 antibody is not suitable for immunofluorescence detection in testicular tissue, to better evaluate the functional location of PAN2, we first overexpressed exogenous PAN2 fused with mCherry in HeLa cells and found that it was mainly localized in the cytoplasm (Fig. 1c). To verify whether PAN2 was also localized in the testis, we used the nuclear-cytoplasm separation method to obtain the nuclear and cytoplasmic fractions of the testes of adult mice. Western blotting showed that PAN2 was enriched in the cytoplasm of testicular cells (Fig. 1d). Based on published transcriptome data<sup>37,38</sup>, we examined the expression of *Pan2* and *Pan3* in the first spermatogenic wave and at different stages of sperm development. *Pan2* and *Pan3* were found to be continuously expressed in the first spermatogenic wave. However, at different stages of sperm development, *Pan2* was expressed at higher levels in the leptotene and zygotene stages, and then showed a downward trend, while *Pan3* was continuously expressed at high levels in the later stages of sperm development (Fig. 1e, f). In addition, we performed FACS to isolate mouse spermatogenic cells from wild-type (WT) adult male testes at five developmental stages: leptotene (L), zygotene (Z), pachytene (P), diplotene (D), metaphase II (MII) phase spermatocytes, and RS. Western blotting results showed that PAN2 was expressed continuously during spermatogenesis but showed a gradual downward trend. This is consistent with transcriptome data (Fig. 1g). These results reveal that PAN2 is highly expressed in the cytoplasm of testicular cells, suggesting that PAN2 plays a role in spermatogenesis.

To study the physiological functions of PAN2, we crossed *Pan2*-floxed mice with *Stra8-Cre* knock-in mice to obtain *Pan2*<sup>fl/fl</sup>; *Stra8-Cre* mice, in which *Pan2* is specifically inactivated in germ cells before

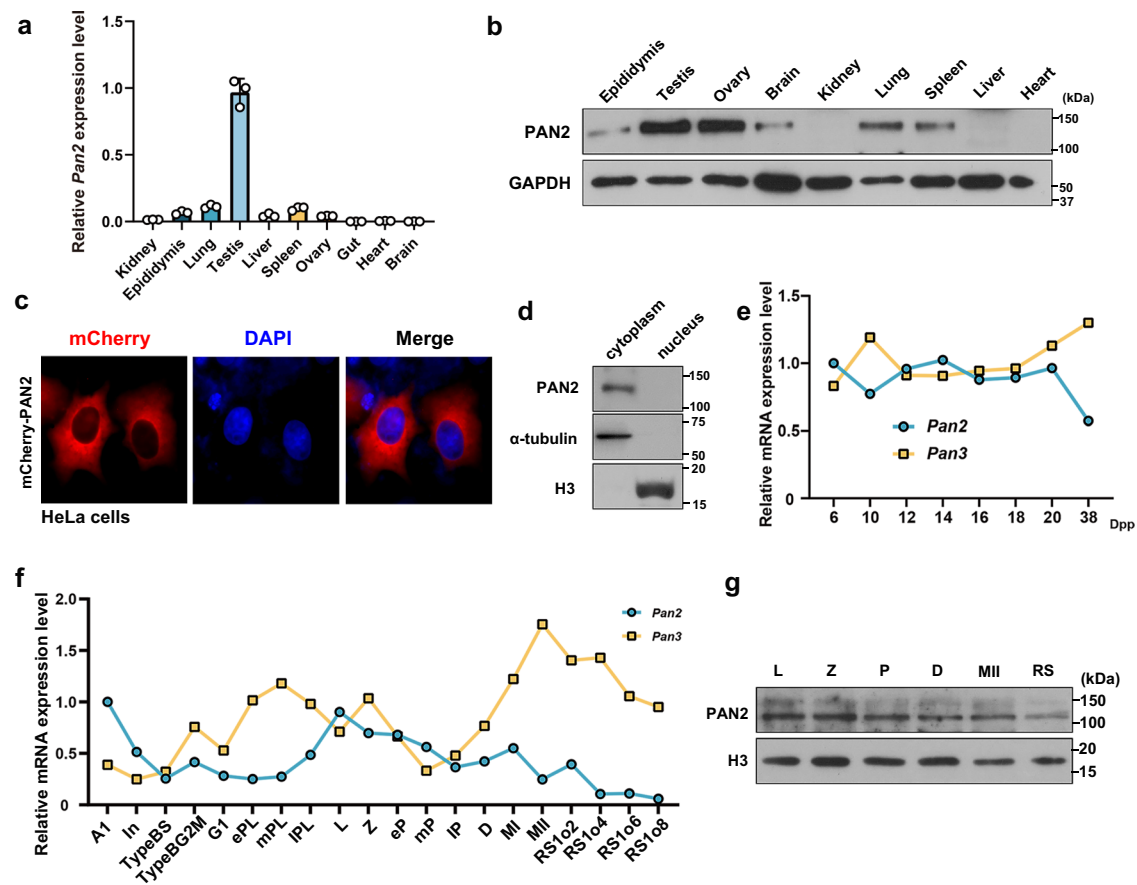


**Fig. 1 | The expression of PAN2 in multiple tissues and male germ cells.**

**a** Reverse transcription-quantitative polymerase chain reaction (RT-qPCR) showing the relative mRNA expression levels of *Pan2* in multiple mouse tissues.  $n = 3$ . Error bars indicate the standard error of the mean (SEM). **b** Western blotting results of PAN2 in mouse somatic tissues. GAPDH was used as a loading control.

**c** Immunofluorescence results showing localization of exogenous PAN2 in HeLa cells. **d** Western blotting analysis of PAN2 protein levels in the cytoplasm and nucleus from adult WT mouse testes.  $\alpha$ -tubulin and H3 were used as loading controls. **e** RNA-seq data showing the relative mRNA expression levels of *Pan2* and *Pan3* in mouse testes on different days postpartum (dpp) during the first wave of spermatogenesis. **f** RNA-seq data showing the relative mRNA expression levels of *Pan2* and *Pan3* in the spermatocytes and spermatids at different developmental stages (A1 type A1 spermatogonia, In intermediate spermatogonia, BS S phase type

B spermatogonia, BG2 G2/M phase type B spermatogonia), preleptotene spermatocytes (G1 G1 phase preleptotene, eP1 early S phase preleptotene, mPL middle S phase preleptotene, IPL late S phase preleptotene), meiotic cells (L leptotene, Z zygotene, eP early pachytene, mP middle pachytene, IP late pachytene, D diplotene, MI metaphase I, MII metaphase II), and round spermatids (RSo2 steps 1-2 spermatids, RSo4 steps 3-4 spermatids, RSo6 steps 5-6 spermatids, RSo8 steps 7-8 spermatids). **g** Western blotting for PAN2 in spermatogenic cells isolated from adult WT mice using fluorescence-activated cell sorting (FACS) (L, leptotene; Z, zygotene; P, pachytene; D, diplotene; MII, metaphase II; RS, round spermatids). H3 was used as a loading control. Representative results shown in (**b**, **d**, **g**) were obtained from at least three independent experiments with similar results. Source data (**b**, **d**, **g**) are provided as a Source Data file.

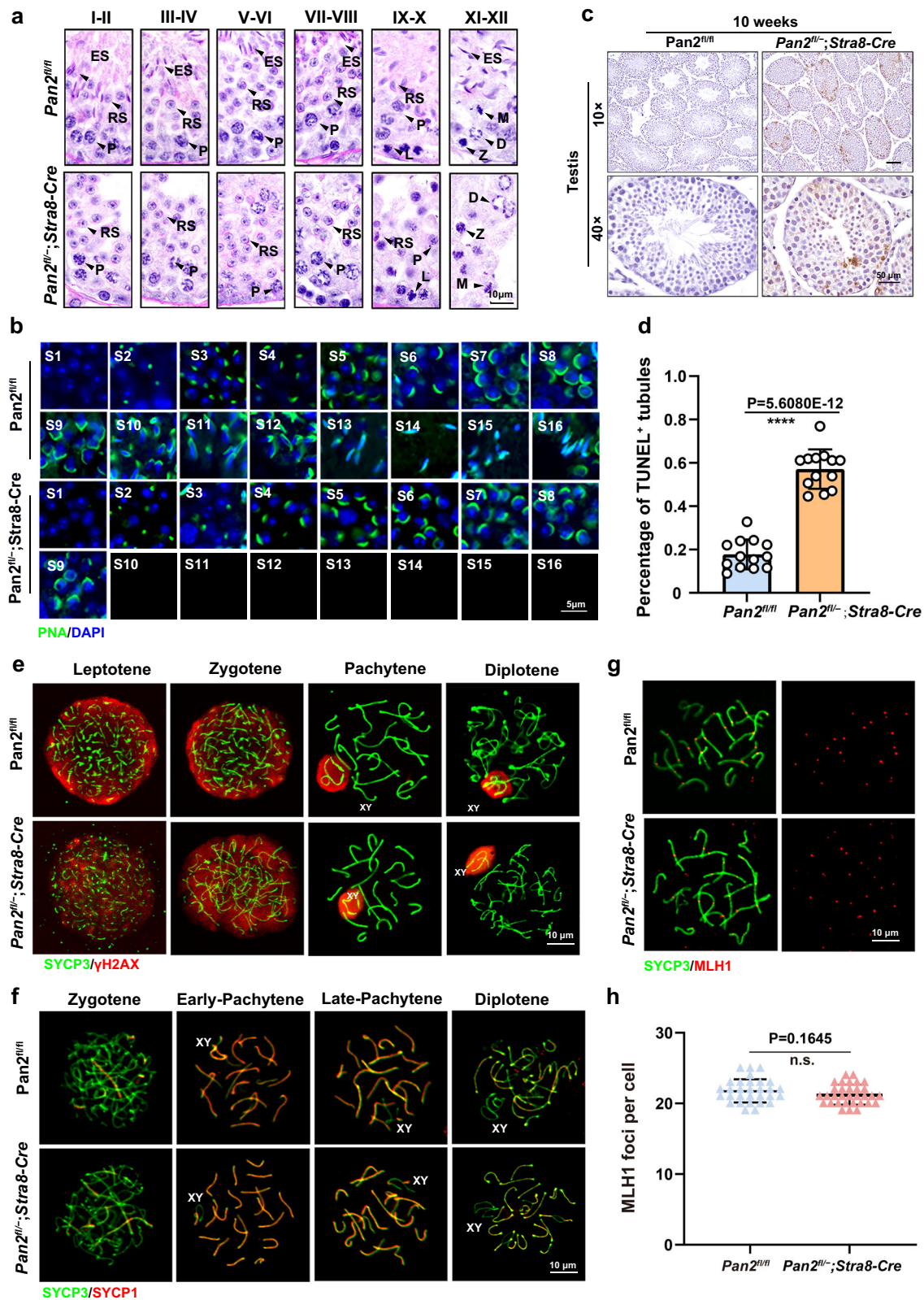
entering meiosis (Fig. 2a). Western blotting results showed that PAN2 protein was not observed in *Pan2*<sup>-/-</sup>; *Stra8-Cre* spermatocytes, while PAN2 expression was normal during the control period (Fig. 2b), indicating that *Pan2* was effectively deleted in *Pan2*<sup>-/-</sup>; *Stra8-Cre* mouse spermatocytes. Control male mice (*Pan2*<sup>+/+</sup> and *Pan2*<sup>+/fl</sup> littermate males) and *Pan2*<sup>-/-</sup>; *Stra8-Cre* males were mated with wild-type females for 6 months. The results showed that *Pan2*<sup>-/-</sup>; *Stra8-Cre* male mice were completely infertile (Fig. 2c). Three weeks after birth, there was no significant difference in the testicular weight between *Pan2*<sup>-/-</sup>; *Stra8-Cre* mice and control mice. However, starting from the 4<sup>th</sup> week, the testicular weight of *Pan2*<sup>-/-</sup>; *Stra8-Cre* mice was significantly lower than that of the control mice (Fig. 2d, e). H&E analysis revealed that no elongated sperm were found in the seminiferous tubules of *Pan2*<sup>-/-</sup>; *Stra8-Cre* mice, and no mature sperm were found in the epididymis (Fig. 2f-h). In addition, immunofluorescence staining showed DDX4 expression (a germ cell marker), but no SYCP3 signal (a meiotic cell marker) in the epididymis of *Pan2*<sup>-/-</sup>; *Stra8-Cre* mice at 10 weeks, indicating that germ cells in the epididymis of *Pan2*<sup>-/-</sup>; *Stra8-Cre* mice were round spermatids that had completed meiosis. These results

illustrated that PAN2 was required for spermatogenesis and male fertility in mice (Fig. 2i).

### **Pan2**-deletion results in germ-cell apoptosis and abnormal spermiogenesis

To trace the time point at which spermatocytes became abnormal in *Pan2*<sup>-/-</sup>; *Stra8-Cre* mice, testicular samples were collected at 21, 28, and 35 days postpartum (dpp) for H&E staining. Morphological analysis showed that there was no difference between *Pan2*<sup>-/-</sup>; *Stra8-Cre* and control mice at 21 dpp. However, *Pan2*<sup>-/-</sup>; *Stra8-Cre* mice did not show elongated sperm in the seminiferous tubules, which were significantly different from those in control mice at 28 dpp. At 35 dpp, elongated sperm were not observed in *Pan2*<sup>-/-</sup>; *Stra8-Cre* mice (Supplementary Fig. 1a). Therefore, PAN2 is essential for the development of the first spermatogenic wave in mice. Haploid sperm development in mice is divided into 16 stages (steps 1–16). Normally, during the differentiation of spermatids, proacrosomal vesicles are formed (step 2–3), fused into a single acrosomal vesicle that attaches to the nuclear surface of the RS (step 4), and spread further over the nuclear surface (step 5–16). As





shown in Fig. 3a, testicular sections from 8-week-old WT males contained spermatids at all stages of differentiation. RS in adult *Pan2<sup>fl/fl</sup>;Stra8-Cre* testes contained periodic acid Schiff (PAS, which specifically labels acrosomal glycoproteins)-positive proacrosomal vesicles (steps 2-3) and flattened acrosomal vesicles; however, elongating spermatids and later stages were not observed, indicating that RS in *Pan2<sup>fl/fl</sup>;Stra8-Cre* mice was arrested at steps 8-9 (Supplementary

Fig. 1b). Immunostaining with the acrosome marker peanut agglutinin (PNA) confirmed the complete absence of spermatids beyond step 8-9 in *Pan2<sup>fl/fl</sup>;Stra8-Cre* mice, but there were no significant abnormalities in the acrosome structure (Fig. 3b).

Terminal deoxynucleotidyl transferase dUTP nick-end labeling (TUNEL) revealed an increased number of apoptotic cells in the tubules of *Pan2<sup>fl/fl</sup>;Stra8-Cre* testes (Fig. 3c), with approximately 60% of

**Fig. 3 | *Pan2*<sup>fl</sup>;*Stra8-Cre* mice showed germ-cell apoptosis and abnormal spermiogenesis.** **a** Periodic acid-Schiff (PAS)-hematoxylin staining of seminiferous tubules from WT and *Pan2*<sup>fl</sup>;*Stra8-Cre* mice. Scale bar: 10  $\mu$ m. **b** Immunofluorescence analysis of PNA in spermatids from WT and *Pan2*<sup>fl</sup>;*Stra8-Cre* mice. Scale bar: 5  $\mu$ m. **c** Terminal deoxynucleotidyl transferase dUTP nick-end labeling (TUNEL) staining of testicular sections of WT and *Pan2*<sup>fl</sup>;*Stra8-Cre* mice. Scale bar: 500  $\mu$ m (upper panels) and 50  $\mu$ m (lower panels). **d** Quantification of the proportion of TUNEL-positive tubules in the testes. \*\*\*\* $P < 0.0001$  by two-tailed Student's *t*-test.  $n = 13$ . Error bars indicate the standard error of the mean (SEM). **e** Immunofluorescence analysis of SYCP3 and  $\gamma$ H2AX in chromosome spreads of

spermatocytes from 10-week-old WT and *Pan2*<sup>fl</sup>;*Stra8-Cre* mice. Scale bar: 10  $\mu$ m. **f** Immunofluorescence analysis of SYCP3 and SYCP1 in chromosome spreads of spermatocytes from 10-week-old WT and *Pan2*<sup>fl</sup>;*Stra8-Cre* mice. Scale bar: 10  $\mu$ m. **g** Immunofluorescence analysis of SYCP3 and MLH1 in chromosome spreads of pachytene spermatocytes from 10-week-old WT and *Pan2*<sup>fl</sup>;*Stra8-Cre* mice. Scale bar: 10  $\mu$ m. **h** Average numbers of MLH1 foci in each pachytene spermatocyte. Two-sided Student's *t*-tests. n.s. non-significant.  $n = 30$ . Representative results shown in (a–c, e–g) were obtained from at least three independent experiments with similar results.

the mutant tubules containing TUNEL-positive cells (Fig. 3d). These results indicated that PAN2 deficiency led to developmental arrest and apoptosis in RS cells.

We observed that *Pan2*-conditional-knockout mice contained spermatocytes that could enter meiosis. We further analyzed the proportions of haploid, diploid, and tetraploid spermatocytes in *Pan2*<sup>fl</sup>;*Stra8-Cre* and WT testes using FACS. The results indicated that the proportion of diploid and tetraploid spermatocytes in *Pan2*<sup>fl</sup>;*Stra8-Cre* testes was normal; however, the number of haploid spermatocytes was reduced (Supplementary Fig. 1c, d). Additionally, size-based FACS analysis of RS and elongated spermatids revealed a significant decrease in the number of elongated spermatids (Supplementary Fig. 1e, f). Histological analysis revealed no significant difference in spermatogenesis during meiotic prophase I between control and *Pan2*<sup>fl</sup>;*Stra8-Cre* mice. To confirm this result, we identified different stages of meiotic prophase I by staining testes tissue sections for phosphorylated H2AX ( $\gamma$ H2AX), a marker of unrepaired DNA lesions and the sex body in pachynema, and SYCP3, a component of the synaptonemal complex. The results showed that all stages existed in the spermatocyte nuclei of the control and *Pan2*<sup>fl</sup>;*Stra8-Cre* mouse testes (Supplementary Fig. 1g). We further examined  $\gamma$ H2AX and SYCP3 on chromosome spreads from spermatocytes in control and *Pan2*<sup>fl</sup>;*Stra8-Cre* mice (Fig. 3e). Statistical analysis showed that the lack of PAN2 did not cause abnormal spermatocyte development at the leptotene, zygotene, pachytene, or diplotene stages (Supplementary Fig. 1h).

In addition, we examined chromosomal synaptic processes using nuclear spreading and immunofluorescence staining for SYCP3 and SYCP1, which are important components of the synaptonemal complex. The signals were similar between control and *Pan2*<sup>fl</sup>;*Stra8-Cre* mice at the pachytene stage (Fig. 3f). MLH1 foci were normally detected in *Pan2*-deleted pachytene spermatocytes (Fig. 3g, h), indicating that *Pan2*-deletion did not affect crossover formation. These results demonstrated that *Pan2*-deletion has no effect on the prophase of meiosis I.

### ***Pan2* deletion has a slight impact on the transcriptome in RS**

To investigate the molecular role of PAN2 in spermatogenesis, we used FACS to separate MII-stage spermatocytes and RS cells. MII spermatocytes were identified based on SYCP3 and DDX4 staining and characteristic metaphase morphology. RS and ES were distinguished by nuclear morphology and acrosome status. For RS, the purity was consistently 90.24 % across all biological replicates; MII fractions also reached 85.94 % purity (Supplementary Fig. 1i–k). Smart-seq2 was further used to construct libraries and perform high-throughput transcriptome sequencing (Fig. 4a). Gene expression levels were quantified as FPKM (fragments per kilobase of transcripts per million mapped reads), after which calibration was performed between different samples using the External RNA Controls Consortium (ERCC) spike-in. Each sample group had at least three biological replicates, and a high correlation was observed between the replicate measurements (Supplementary Fig. 2a, b).

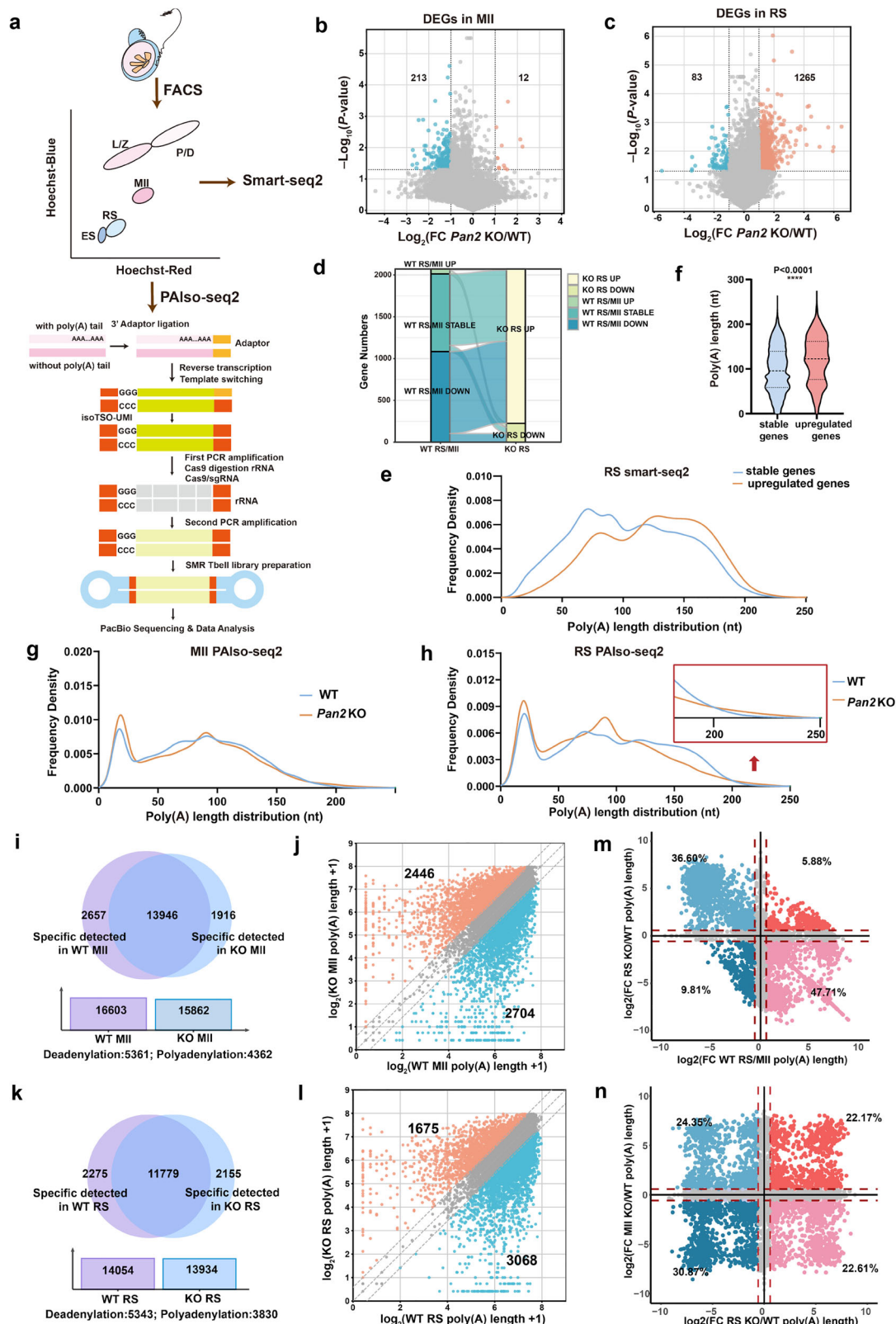
Transcriptome profiling results showed that the loss of *Pan2* in the MII phase resulted in the downregulation of 213 genes and the

upregulation of 12 genes (Fig. 4b). The effect on the transcriptome at this stage was relatively modest. However, at the RS phase, deletion of *Pan2* resulted in the downregulation of 82 genes and upregulation of 1265 genes (Fig. 4c). The Sankey diagram shows the dynamics of differentially expressed transcripts from the MII to RS stages. Most of the transcripts that were downregulated from MII to RS in WT mice were upregulated in the RS of *Pan2*-deletion cells (90.40%). In addition, a subset of the transcripts stably expressed from MII to RS in the WT was upregulated (91.92%) or downregulated (8.08%) in the RS of *Pan2*-deletion cells (Fig. 4d). These results indicate that *Pan2* deletion has a slight effect on the transcriptome during the MII and RS periods.

The role of PAN2 as a key mRNA deadenylation enzyme in the regulation of spermatogenesis remains unclear. To further investigate the molecular mechanisms underlying the arrest of spermatogenesis due to *Pan2*-deletion, we analyzed changes in the mRNA poly(A) tail using PAIso-seq2 (see above). We obtained highly pure MII stage spermatocytes and RS using fluorescence-activated cell sorting (FACS), extracted high-quality total RNA, and then purified the mRNA by enrichment of the poly(A) tail, followed by RT to synthesize full-length cDNA and PCR amplification to construct a sequencing library. Finally, long-read sequencing was performed using the PacBio platform to obtain the complete transcript structure information for analysis. The data showed that a reliable number of circular consensus sequences (CCS) reads was obtained with high correlation within the sample group (Supplementary Fig. 2c–e). Additionally, the poly(A) tail lengths of some genes highly expressed at the protein level during RS aligned with this trend (Supplementary Fig. 2f). These results indicated that the data from PAIso-seq2 were reliable. The comparison of poly(A) tail length distributions between stable and upregulated genes revealed that upregulated genes generally tended to have longer poly(A) tails in WT mice (Fig. 4e, f).

### ***Pan2*-deletion results in an increased number of long-tail mRNAs and global tail length disorders during spermiogenesis**

The mRNA poly(A) tail undergoes dynamic changes during normal spermatogenesis. The results of PAIso-seq2 showed that, except for some shorter tails (less than 50 nt) with a relatively high proportion, the poly(A) tail length distribution of spermatocyte mRNA in the MII phase was mainly concentrated at 50–130 nt, while the tail length distribution in the RS period was more broadly distributed (Supplementary Fig. 3a, b). The proportion of mRNAs with poly(A) tails greater than 150 nt increased when MII phase spermatocytes switched to RS in mice (Supplementary Fig. 3c). We further examined the effect of *Pan2* deletion on the poly(A) tail of mRNA during spermatogenesis. At the MII stage, the proportion of mRNA with different poly(A) tails in *Pan2*-deficient spermatocytes was similar to that in WT spermatocytes (Fig. 4g), but in the RS stage, there were significant differences in the proportion of mRNA with different poly(A) tails. The proportion of genes with long poly(A) tails was greater in *Pan2*-deleted RS than in WT RS. A clear observation is that in WT, there is a change in the overall distribution of mRNA poly(A) tails from the MII to RS period, which appears to be lost after the loss of *Pan2* (Fig. 4h). To assess this possibility, we employed PAIso-seq2 to detect the differentially polyadenylated genes (DPGs) in *Pan2*-deleted MII phase spermatocytes and



RS. As expected, the poly(A) residues of some DPGs in *Pan2*-deleted MII phase spermatocytes (Fig. 4i, j) and RS (Fig. 4k, l) were abnormally elongated. However, abnormally shortened tails have also been observed in some DPGs. In both MII phase spermatocytes and RS, detailed transcript analysis exhibited a bias toward longer poly(A) tails in WT mice, whereas the tail lengths of the polyadenylation genes were shortened under the same conditions (Supplementary Fig. 3d, e). We

further divided the segments by tail length, thereby comparing the polyA tail lengths in WT and *Pan2*<sup>fl/-</sup>; *Stra8*-Cre mice. Through a segment-wise comparison, we observed significant poly(A) tail removal and addition at various segment lengths during the MII stage (Supplementary Fig. 3f, g). The RS stage showed a similar pattern, indicating that the overall effect of *Pan2* deletion on tail homeostasis was a broad-spectrum effect (Supplementary Fig. 3h, i).

**Fig. 4 | *Pan2* deletion resulted in disordered mRNA tail length.** **a** Schematic diagram of Smart-seq2 and PALso-seq sequencing. **b, c** Volcano plots show the number of significantly differentially expressed genes (DEGs) in MII phase spermatocytes (**b**) and RS (**c**) from WT and *Pan2*<sup>fl/fl</sup>;*Stra8-Cre* mice. The *P* threshold (0.05) and log2FC threshold ( $\pm 1$ ) are reported in gray horizontal and vertical lines, respectively. FC, fold change. *n* = 3 biological replicates per group. Two-sided Student's *t*-tests. **d** Sankey diagram showing the flow patterns of downregulated, upregulated, and stable transcripts in RS from WT and *Pan2*<sup>fl/fl</sup>;*Stra8-Cre* mice. Each rectangle represents a gene category. FC =  $\pm 2$ . *n* = 3 biological replicates per group. **e** Distribution graph of mRNA poly(A) tail length of upregulated and stable transcripts in *Pan2*-deleted versus WT RS. *n* = 3 biological replicates per group. **f** Violin diagram of mRNA poly(A) tail length of upregulated and stable transcripts in *Pan2*-deleted versus WT RS. \*\*\*\**P* < 0.0001 by two-tailed Student's *t*-test. **g, h** Distribution graph of mRNA poly(A) tail length in MII phase spermatocytes (**g**) and RS (**h**) in WT and *Pan2*<sup>fl/fl</sup>;*Stra8-Cre* mice. *n* = 3 biological replicates per group. **i** Venn diagram

displaying the overlapping genes detected in WT and *Pan2*-deleted spermatocytes at the MII stage. The overlap represents genes with non-zero poly(A) tail lengths in both WT and *Pan2*-deleted MII phase spermatocytes, which were selected for further analysis of the polyadenylation changes in (**j**). *n* = 3 biological replicates per group. **j** Scatter plot comparing the poly(A) tail lengths of mRNAs in *Pan2*-deleted versus WT MII phase spermatocytes. Results are from three independent experiments. **k** Venn diagram displaying the overlapping genes detected in WT and *Pan2*-deleted RS. The overlap represents genes with non-zero poly(A) tail lengths in both WT and *Pan2*-deleted RS, which were selected for further analysis of the polyadenylation changes in (**l**). *n* = 3 biological replicates per group. **l** Scatter plot comparing the poly(A) tail lengths of mRNAs in *Pan2*-deleted versus WT RS. *n* = 3 biological replicates per group. **m** Scatter plot comparing DPGs in *Pan2*-deleted versus WT RS and DPGs in WT RS versus MII phase spermatocytes. *n* = 3 biological replicates per group. **n** Scatter plot comparing DPGs in *Pan2*-deleted versus WT RS and MII phase spermatocytes. *n* = 3 biological replicates per group.

Next, we observed that some genes typically undergo tail shortening from MII to RS in WT samples; however, following *Pan2* deletion, these tails were abnormally elongated. Additionally, the poly(A) tails of some genes, which were extended, appeared abnormally shortened (Fig. 4m), but there was no correlation between the DPGs of MII and RS after *Pan2* deletion (Fig. 4n). This indicated that the change in mRNA poly(A) tail from MII phase to RS in WT under normal physiological conditions does not occur following *Pan2* deletion. These results indicated abnormal deadenylation and polyadenylation in both MII phase spermatocytes and RS.

### PAN2 regulates key proteins involved in translation and spermiogenesis

Translation is critical in spermiogenesis, and important proteins need to be expressed to regulate a series of important physiological and biochemical processes. We found that *Pan2* deletion can cause mRNA poly(A) homeostasis disorders, but whether this interferes with subsequent translation remains unknown. To further explore the molecular mechanism by which *Pan2* deletion leads to spermatogenesis disorders, we used mass spectrometry to analyze the effect of *Pan2* deletion on translation. The data demonstrated high consistency within the groups (Supplementary Fig. 4a, b), and we validated the expression patterns of selected proteins using western blotting, confirming the reliability of the mass spectrometry results (Supplementary Fig. 4c). The fold change (FC) in the amount of differential expression level exceeding 2.5 and less than 0.4 (*Pan2* KO/WT) was regarded as the threshold for significant upregulation and downregulation, respectively. Mass spectrometry results showed that the expression levels of 1884 proteins were significantly decreased in *Pan2*-deleted RS compared to WT spermatids, while only 111 proteins were upregulated (Fig. 5a, b). Gene Ontology (GO) analysis of the downregulated proteins showed that their functions were closely related to spermatogenesis and translation (Fig. 5c). In addition, detailed functional analysis of the downregulated proteins revealed that they were related to cilium assembly, microtubule cytoskeleton, chromatin remodeling, and apoptotic (Fig. 5d). *Pan2* deletion reduces the levels of several key proteins during spermatogenesis. These findings were integrated with the PALso-seq2 results for further analysis. In total, 144 and 369 genes showed decreased protein expression levels in the polyadenylation and deadenylation genes, respectively (Fig. 5e). Additionally, genes related to male fertility were screened, and a heat map was generated to illustrate the changes in poly(A) tail length (Fig. 5f). We further verified using RIP-qPCR that some of these genes were directly regulated by endogenous PAN2. *Wdfy3*, which had a short poly(A) tail, as measured in PALso-seq2, and did not change significantly after *Pan2* loss, was used as a negative control (Supplementary Fig. 4d). We further confirmed the interaction between endogenous PAN2 and PAN3 in the testis using endogenous IP experiments. Specifically, *Prmt1*, *Nek1*, *Armc3*, *Rnf216*, and *Ube2g1* were

identified as PAN3-targeted regulatory genes by RIP-qPCR (Supplementary Fig. 4e, f). This indicates that PAN3 is also involved in the regulation of some genes by PAN2. Furthermore, the poly(A) tail assay confirmed that *Nek1* and *Armc3* had significantly extended poly(A) tails in *Pan2*-deletion RS (Fig. 5g, h). NEK1 deletion leads to severe fertility impairment in males and is involved in regulating the redistribution of adhesins in mouse spermatocytes<sup>39</sup>. ARMC3 is essential for spermatogenesis, and homozygous splicing variants of ARMC3 cause asthenospermia and flagellar disorganization in consanguineous families<sup>40</sup>. Moreover, the poly(A) tail assay analysis of *Herc2* and *Rnf216* revealed that the poly(A) tail lengths of these genes were significantly shortened in *Pan2*-deletion RS (Fig. 5i, j). RNF216, an E3 ubiquitin ligase, has been reported to be essential for spermatogenesis and male fertility in mice<sup>41</sup>. It's worth mentioning that the transcriptome data of the above genes showed no significant change in their mRNA levels after *Pan2* deletion, indicating that the decrease in their protein levels was not caused by a decrease in mRNA levels (Supplementary Fig. 4g). Disruption of the poly(A) tail length in genes encoding these proteins, which are closely associated with spermatogenesis and male reproduction, results in a significant decrease in protein levels and, ultimately, causes abnormal spermatogenesis.

### PAN2 interacts with translation-related proteins

We confirmed that, after the deletion of *Pan2* in the mouse RS, some proteins were directly regulated by the poly(A) tail, resulting in a decrease in protein levels. However, in addition to this, the expression levels of a large number of proteins were significantly reduced. We further explored whether *Pan2* uses other mechanisms for regulating translation. Therefore, immunoprecipitation coupled with mass spectrometry (IP-MS) was performed to identify PAN2-interacting proteins. The anti-PAN2 antibody was conjugated to protein A beads. Potential PAN2-binding proteins in the testis fragment suspension were enriched and screened using mass spectrometry (Fig. 6a). We compared the proteins identified by IP-MS with the protein profiles during the WT RS stage, and found that 70.99% of the proteins were expressed during the RS period. In addition to the potential PAN2-interacting proteins (*n* = 678) identified exclusively in the endogenous IP group, proteins with an FC exceeding the amount of differential expression between the *Pan2* IP group and IgG group were similarly classified as candidate PAN2-interacting proteins in the testes. We ultimately identified 785 potential interacting proteins that PAN2 might bind to during the RS period (Fig. 6b, c). GO analysis indicated that the PAN2-interacting proteins were related to translation and mRNA processing. We focused on these proteins in subsequent experiments (Fig. 6d, e). We verified the endogenous IP results using western blotting and found that endogenous PAN2 interacted with EIF5A, EIF4A1, and EIF4E. Additionally, PAN2 interacted with PABPC1 (Fig. 6f and Supplementary Fig. 4h). PABPC1 is closely associated with mRNA translation; therefore, we confirmed an RNA-independent

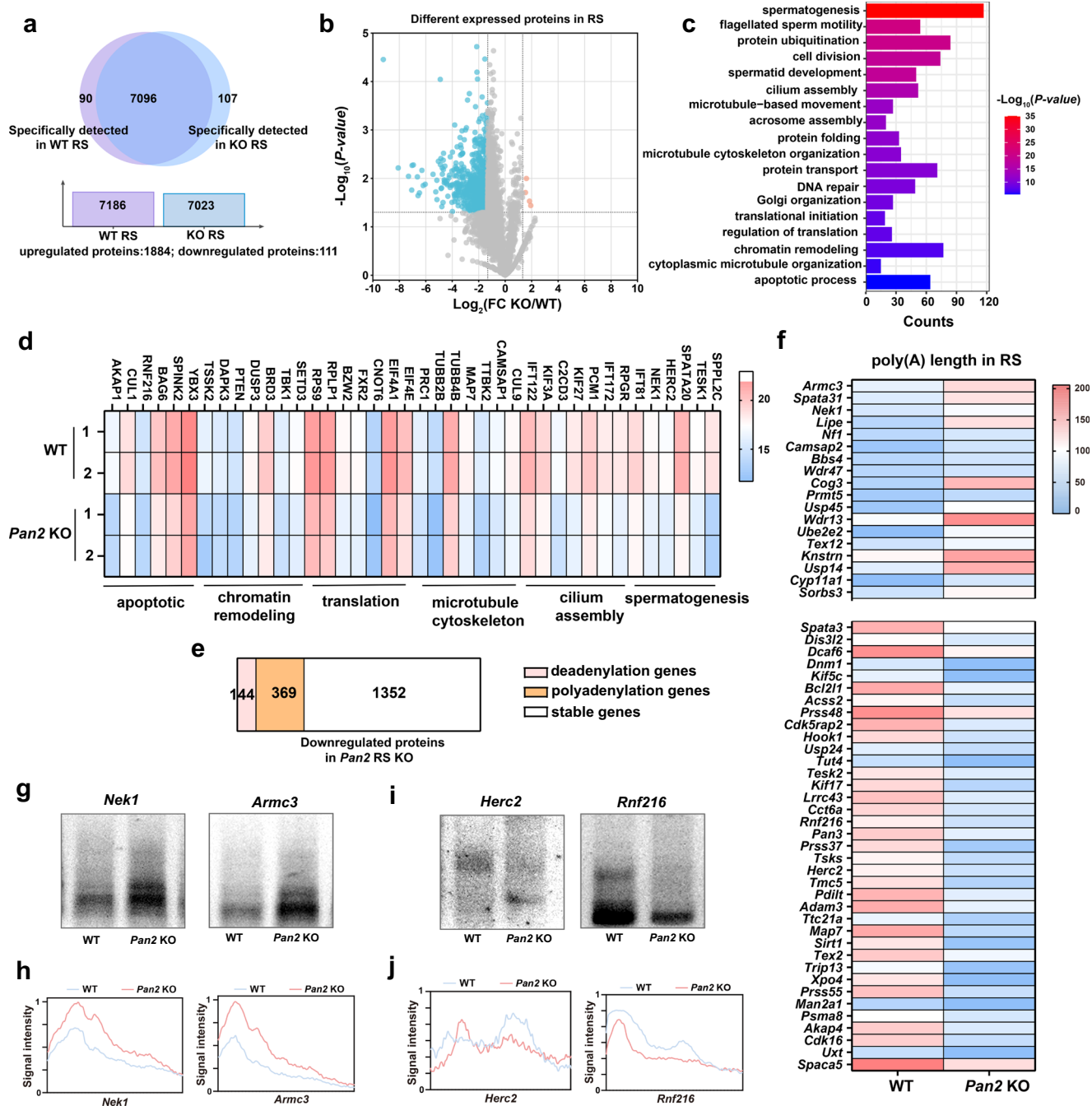
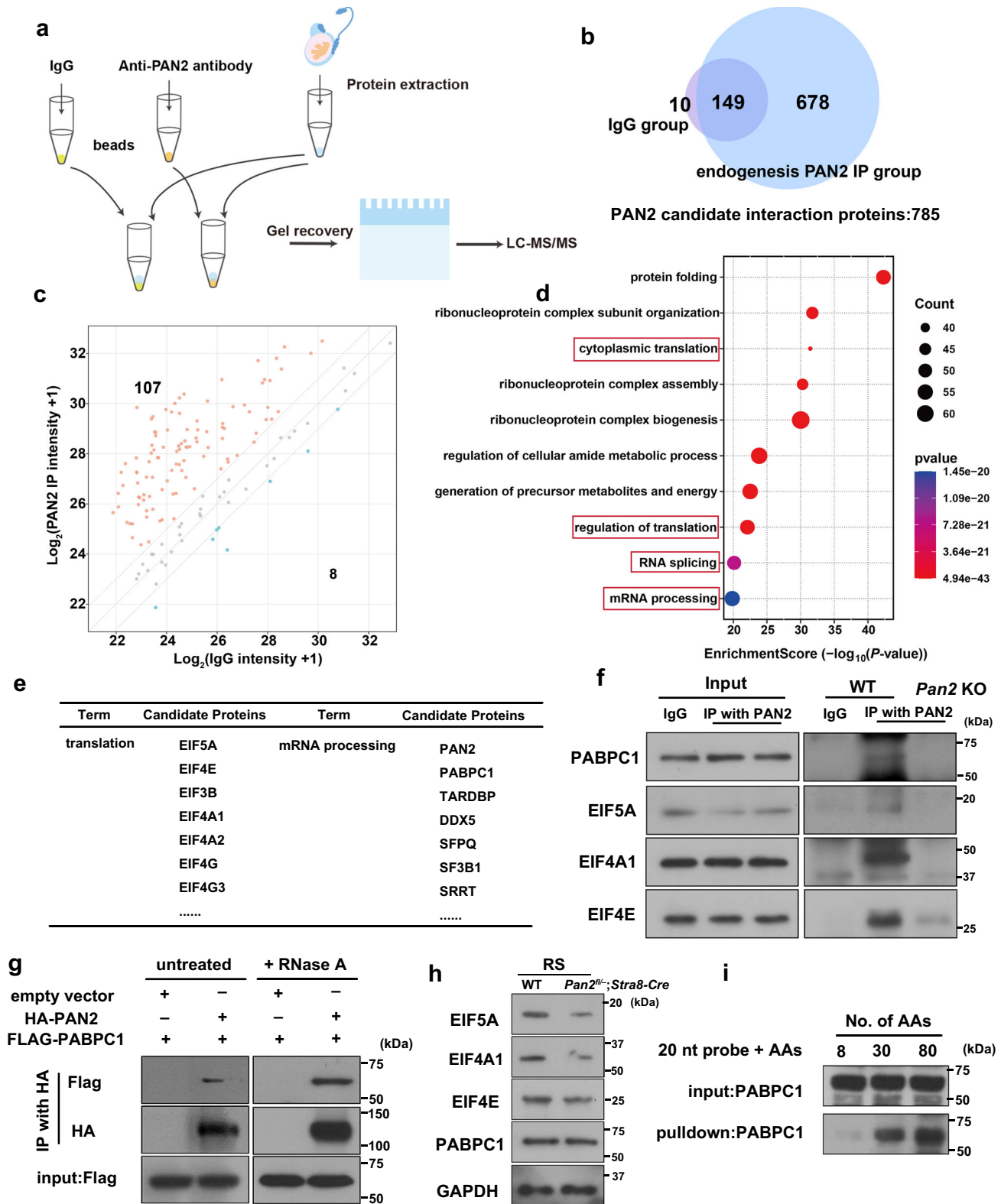


**Fig. 5 | Proteomics analysis verified that PAN2 participated in the regulation of translation during spermatogenesis.** **a** Venn diagram displaying the overlapping proteins detected in WT and *Pan2*-deleted RS. The overlap represents proteins with non-zero quantity in both WT and *Pan2*-deleted RS, which were selected for further analysis in **(b)**. **b** Volcano plot shows the downregulated and upregulated proteins in *Pan2*-deleted RS. The *P* threshold (0.05) and FC threshold ( $\pm 2.5$ ) are reported in gray horizontal and vertical lines, respectively. FC, fold change. Two-sided Student's *t*-tests. **c** Gene Ontology (GO) analysis of downregulated proteins in *Pan2*-

deleted RS. Two-sided Student's *t*-tests. **d** Heat map showing the expression level of downregulated proteins in WT and *Pan2*-deleted RS. **e** Proportion plot showing the proportion of deadenylation and polyadenylation transcripts in the downregulated proteins in the WT and *Pan2*-deleted RS. **f** Heat map showing the poly(A) tail length of partially overlapping genes in **(e)**. **g, h** Poly(A) tail length of transcripts in the WT and *Pan2*-deleted RS were evaluated using poly(A) tail assays. **i, j** Relative signal intensity (*y*-axis) and PCR product length according to mobility (*x*-axis).

interaction between PAN2 and PABPC1 in 293T cells (Fig. 6g). Simultaneously, by combining the results of mass spectrometry and western blotting, we found that the protein levels of EIF5A, EIF4A1, and EIF4E were also decreased in *Pan2*-deficient RS, but the protein level of PABPC1 remained stable (Fig. 6h). And the transcriptomic data showed that the mRNA levels of these proteins did not change significantly after *Pan2* deletion, indicating that the decrease in their protein levels was not due to a decrease in mRNA levels (see above). Furthermore,

because *Pan2* deletion resulted in an increase in mRNA levels with longer poly(A) tails, we assessed whether longer poly(A) tails occupied more PABPC1. RNA probes with poly(A) tails of different lengths were designed for pull-down experiments. The results showed that RNA probes with longer tails bound more PABPC1 (Fig. 6i). This interaction suggested that PAN2 influenced translation through a functional relationship with PABPC1. Therefore, PAN2 may regulate translation during spermiogenesis by interacting with these proteins.



**PAN2 and PABPC1 function in concert to modulate translation during the RS stage**

As the mRNA poly(A) tail itself is also closely related to mRNA translation, we further examined the effect of *Pan2* deletion on the translome at RS stage by low input Ribo-seq (Ribo-lite). The Ribo-lite library construction protocol for flow-sorted spermatocytes (RS) begins with cell lysis to release and stabilize ribosome-nascent chain complexes. This is followed by digestion with RNase I to cleave mRNA

regions not protected by ribosomes, yielding ribosome-protected fragments (RPFs). The monomeric ribosomes are then isolated via ultracentrifugation through a sucrose cushion, and the RPFs are size-selected and enriched using label-free polyacrylamide gel electrophoresis. The final library is constructed through a series of steps, including T4 PNK end repair, adapter ligation, cDNA synthesis, and PCR amplification (Fig. 7a). The results showed that effective analytical fragments were obtained and good reproducibility was achieved

**Fig. 6 | PAN2 interacted with PABPC1, and longer poly(A) tails bound more PABPC1.** **a** Schematic representation of immunoprecipitation coupled with mass spectrometry (IP-MS) analysis of PAN2 in the testis. **b** Venn diagram displaying the overlapping proteins detected in the IgG and endogenous PAN2 IP groups. The overlap represents proteins with non-zero intensity in both groups, and these were selected for further analysis of protein levels in (c). Results are from two independent experiments. **c** The scatter plots showing the fold relationship between the PAN2 IP group and the IgG group. The FC threshold ( $\pm 2$ ) is indicated by gray slashes. FC, fold change. Results are from two independent experiments. **d** GO analysis of potential PAN2-interacting proteins, as determined using IP-MS. Two-sided Student's *t*-tests. **e** List of some potential PAN2-interacting proteins related to

translation and mRNA processing. **f** Endogenous immunoprecipitation results showing interactions of PAN2 with translation-related proteins in the RS. **g** Co-immunoprecipitation results showing the interactions between HA-tagged PAN2 and FLAG-tagged PABPC1, with or without RNase A digestion. **h** Western blotting analysis of EIF5A, EIF4A1, EIF4E, and PABPC1 protein levels in WT control and *Pan2*<sup>fl</sup>/*Stras8-Cre* RS. GAPDH was used as a loading control. **i** RNA pull-down results showing PABPC1 protein levels bound by probes with different lengths of poly(A) tails. Representative results shown in (g, i) were obtained from at least three independent experiments with similar results. Source data (g,i) are provided as a Source data file.

(Supplementary Fig. 5a–c). To eliminate the interference of the total mRNA levels, we normalized the ribosome-protected fragment (RPF) counts to the corresponding RNA-seq data to calculate translation efficiency (TE, RPF/mRNA)<sup>42</sup>. This derived metric was then compared between the experimental and control groups to assess the impact of *Pan2* deletion on translational regulation. The fold change (FC) in the amount of differential expression exceeding 1.5 and less than 0.667 (*Pan2* KO/WT) was regarded as the change threshold for a significant up-regulated and down-regulated, respectively. We found 3039 genes with significantly reduced translation efficiency in *Pan2* deletion RS (Fig. 7b). GO analysis showed that these TE down-regulated genes were enriched in spermatid differentiation, spermatid development and cilium, which were consistent with the arrest of sperm development and sperm loss caused by PAN2 deletion (Fig. 7c). The joint analysis of the transcriptome and the mass spectrometry data revealed that their trends of changes were positively correlated, suggesting that the decrease in protein levels was associated with the reduction in translation efficiency. However, although the protein levels of translation-related proteins EIF4A, EIF5A, and EIF4E, which interact with PAN2, decreased, their translation efficiency did not change, suggesting that protein stability was more likely affected (Fig. 7d).

To determine if PAN2-mediated translational regulation involves PABPC1, we performed endogenous RNA immunoprecipitation sequencing (RIP-seq) on testis samples using a PABPC1-specific antibody. This identified 2,728 transcripts (Fold Change  $\geq 3$ , *P*-value  $< 0.05$ ) significantly bound by PABPC1 (Fig. 7e). By jointly analyzing the genes regulated by PABPC1 with the results from Ribo-lite, it was found that after the deletion of *Pan2*, the translation efficiency of the genes targeted by PABPC1 also decreased overall (Fig. 7f). Based on the results of RNA pull down (see above), we hypothesized that PABPC1 would cooperate with PAN2 during the RS period to bind to longer poly(A) tails. Therefore, we analyzed the length of poly(A) tails in the target genes of PABPC1. The results showed that, compared to non-target genes, the poly(A) tails of PABPC1 target genes were significantly longer at RS stage (Fig. 7g). Furthermore, we compared the genes identified by both RIP-seq and PALISO-seq2. Among these genes, 67.05% of the PABPC1 target genes exhibited abnormal elongation or shortening of the poly(A) tail after *Pan2* deletion (Fig. 7h). Moreover, the mRNA expression levels of most PABPC1 target genes did not show significant changes after PAN2 deletion. However, 19.90% of the genes still showed an increase in their transcriptome expression levels after PAN2 deletion (Supplementary Fig. 5d). Additionally, some genes with extended poly(A) tails are also targets of PABPC1, and the expression levels of these genes have also increased (Supplementary Fig. 5e). These results indicate that PABPC1 is potentially involved in the regulation of the translation process by PAN2 at the RS stage.

## Discussion

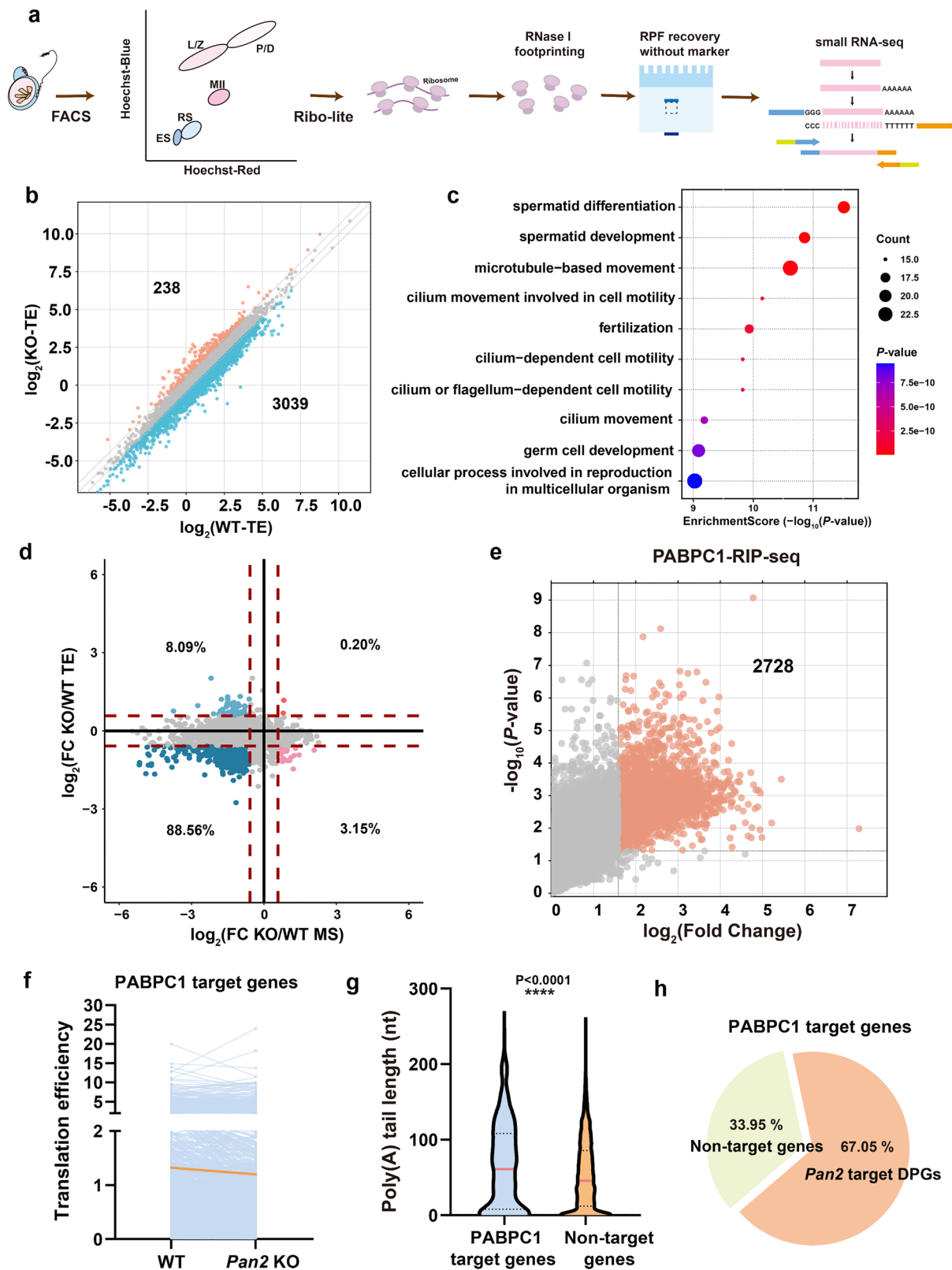
Deadenylation is an important regulatory mode at the RNA level and is involved in most cellular activities and many important physiological and pathological processes. Deadenylases play a central role in this process. As negative regulators of mRNA stability, deadenylase enzymes belong to the 3'-5' exonuclease category. They specifically

catalyze the hydrolysis of the 3' end of the poly(A) tail of RNA and regulate the length of poly(A) tails of mRNA, thereby regulating RNA homeostasis and the degradation process<sup>43</sup>. In this study, we first examined the expression of the deadenylase PAN2 in different tissues and found that it was preferentially expressed in reproductive organs, such as the testes and ovaries. Specific deletion of *Pan2* in male germ cells resulted in impaired spermatogenic transition from round to elongated spermatids, sperm apoptosis, and abnormal adhesion. These phenotypes indicated that PAN2 is a developmentally indispensable protein in male germ cells. Additionally, the use of PALISO-seq2 to investigate poly(A) tails during spermatogenesis allowed us to further explore the dynamics and functions of PAN2-regulated poly(A) tail length in germ cells. We found that the poly(A) tails of mRNAs in *Pan2*-deletion RS were disordered. *Pan2* deletion led to the extension of some mRNA poly(A) tails.

However, the poly(A) tails of some mRNAs were shortened. We speculate that these genes are indirectly regulated by *Pan2*. Because *Pan2* has no ability to bind to RNA, we speculated that there are proteins involved in *Pan2* regulation. The results of IP-MS showed that endogenous PAN2 interacts with PABPC1. PABPC1 is an RNA-binding protein that participates in the polyadenylation and deadenylation processes and is closely related to the regulation of mRNA length. We also verified that longer poly(A) tails showed greater binding to PABPC1. Furthermore, through the combined analysis of RIP-seq and Ribo-lite, we found that the RNAs targeted by PABPC1 also showed a decrease in translation efficiency after the *Pan2* deletion. This indicates that PABPC1 is indeed involved in the process of PAN2 regulation of translation during sperm development. Additionally, we speculated that, when PABPC1 is restricted, the abnormal increase in the levels of mRNAs with long poly(A) tails may interfere with normal polyadenylation and deadenylation by restricting PABPC1, resulting in an overall tail length disorder. However, because sperm cells are difficult to culture in vitro, the specific regulatory mechanisms require further experimental design.

In mammals, chromatin remodeling occurs in spermatogenic cells after meiosis. Histones in the nucleus are gradually replaced by transition proteins and protamine, the nucleus is gradually compressed, and transcriptional activity is gradually silenced<sup>44,45</sup>. When a sperm cell reaches a certain stage of development, mRNA that has been previously transcribed for temporary storage is activated and enters the translation machinery for the synthesis of related proteins, a process known as "transcription-uncoupled translation"<sup>46,47</sup>. Previous studies suggest that the overall translation activity culminates during the late spermatocyte stage and is closely related to sperm formation<sup>48,49</sup>. Therefore, spermiogenesis, the process by which RS differentiates into elongated spermatids and eventually forms spermatozoa, is an excellent model for studying the regulation of poly(A) tail length and translation<sup>50,51</sup>. For example, in *Paip2a/Paip2b* double-knockout mice, where mis-regulated PABP-dependent translation leads to defective elongating spermatids and male infertility<sup>33</sup>.

In our study, *Pan2* deletion does not disrupt meiotic prophase I, as indicated by normal synapsis, recombination markers, and crossover formation ( $\gamma$ H2AX, SYCP1/3, MLH1). Instead, the phenotype first



emerges precisely at the RS-to-elongating spermatid transition, with arrest at steps 8–9 and increased germ-cell apoptosis. This coincidence with the period of maximal translational activities indicates a fundamental defect in the translation regulation rather than any abnormality in the early transcription or meiotic process. A critical question arises as to why *Pan2* deficiency specifically arrests spermatogenesis at step 8–9, despite high PAN2 expression in earlier meiotic

stages. Step 8 marks a pivotal transition where the haploid genome becomes transcriptionally silenced due to chromatin compaction, and cellular development switches to a translation-dependent program driven by stored mRNAs. Our data suggest that PAN2 functions during meiosis to establish an optimal poly(A) tail “set-point” for these stored transcripts. In the absence of PAN2, the fine-tuned homeostasis of poly(A) tails is disrupted. Consequently, the translational burst

**Fig. 7 | *Pan2* deletion results in compromised mRNA translation efficiency during the RS stage.** **a** Ribo-lite sequencing schematic diagram. **b** The scatter plot showing the gene distribution of TE upregulation ( $FC \geq 1.5$ ) and TE downregulation ( $FC \leq 0.667$ ). FC, fold change.  $n = 3$  biological replicates per group. **c** Gene Ontology (GO) analysis of TE downregulation in *Pan2*-deleted RS. Two-sided Student's *t*-tests. **d** The scatter plot showing the correlation between mass spectrometry and Ribo-lite results. **e** The volcano plot showing that PABPC1 binds to RNA ( $FC > 3$ ,  $P$ -value  $< 0.05$ ), and the results are from RIP-qPCR. FC, fold change. Two-sided Student's *t*-tests. The data were calibrated using *Gapdh*.  $n = 3$  biological replicates per

group. **f** Line chart showing the translation efficiency of PABPC1 target genes in WT and *Pan2*-deletion RS. The middle orange line indicates the median expression level.  $n = 3$  biological replicates. **g** Violin plot showing the poly(A) length of the PABPC1 target genes and non-target genes in WT RS. \*\*\*\* $P < 0.0001$  by two-tailed Student's *t*-test. **h** Pie chart showing the proportion of *Pan2* target DPGs among the PABPC1 target genes.  $n = 3$  biological replicates. Representative results shown in panels (f–i) were obtained from at least three independent experiments with similar results. Source data (f–i) are provided as a Source data file.

required for acrosome formation and nuclear elongation at step 8 fails to occur accurately. This phenotype mirrors the translational defects observed in *Paip2a/Paip2b* knockout mice, underscoring that precise poly(A) tail control is the bottleneck for the round-to-elongating spermatid transition.

Our PALso-seq2 data revealed a complex phenotype where *Pan2* deletion caused both aberrant lengthening and shortening of poly(A) tails. We propose a “PABPC1 redistribution model” to explain this duality. Under physiological conditions, the PAN2–PAN3 complex performs the initial trimming of long poly(A) tails. In its absence, a subset of transcripts retains hyper-adenylated tails, which excessively sequester PABPC1 (consistent with our RNA pull-down results). This sequestration may deplete the local pool of free PABPC1, rendering other non-target transcripts vulnerable to unregulated deadenylation by the CCR4–NOT complex or other nucleases. Additionally, we observed that PAN2 loss leads to the destabilization of its partner PAN3 and translation initiation factors (eIF4E, eIF4A1). This multi-dimensional disruption—loss of deadenylase activity, altered PABPC1 distribution, and instability of the translation machinery—culminates in the global translational failure observed in round spermatids. However, in this study, we did not fully elucidate the changes in the binding activity of PABPC1 to the target gene after the deletion of PAN2, due to the limited amount of protein samples available from *Pan2*-deleted spermatids. Further, more rigorous and appropriate technologies are needed to explore this matter.

This disorder is a continuous process that occurs from the MII stage spermatocytes to the RS. At the same time, the levels of most proteins decreased. This also shows that, during spermiogenesis, abnormal prolongation or shortening of the poly(A) tail causes a decrease in translation, thereby interfering with the normal progress of spermiogenesis. This was verified by the MS results. The protein levels of many genes at the RS were decreased after *Pan2* knockout, and these proteins were essential for spermatogenesis-related processes, such as chromatin condensation and cell adhesion.

In addition to *Pan2*, which directly regulates the transcript tail to affect protein translation, there are some proteins for which the levels were downregulated, but not through the influence of the poly(A) tail. We used IP-MS to explore other possible mechanisms by which *Pan2* regulates translation. PAN2 interacts with proteins related to translation initiation in the RS, such as EIF4A and EIF4E. Simultaneously, the expression levels of these proteins were reduced in *Pan2*-deletion RS, but their own translation was not affected. This indicates that *Pan2* may affect the stability of these translation initiation proteins, thereby affecting the translation of many other proteins. Although the stability of these proteins in *Pan2*-deficient RS cannot be directly assessed due to the inability to culture sperm cells in vitro, our data from mass spectrometry and Ribo-lite have ruled out translational-level alterations as a contributing factor. Consequently, this series of translation dysfunctions led to a significant decrease in the expression levels of numerous proteins, ultimately causing a developmental arrest in the spermiogenesis process at the step 8 stage. This further highlights the importance of PAN2 in translation regulation.

Spermatogenesis is a complex process with a series of steps that require fine regulation and is mainly divided into three parts: mitosis,

meiosis, and spermiogenesis. However, enzymes involved in cytoplasmic mRNA degradation are not uniformly involved in the regulation of these processes. CNOT4 and TUT4/7 are involved in the regulating of meiosis<sup>7,11</sup>, while CNOT7 and PAN2 only show physiological functions during spermiogenesis<sup>9</sup>. Following the loss of downstream DIS3L2, developmental abnormalities occur during spermatogonial differentiation<sup>12</sup>. This difference in the regulatory modes at different stages of male spermatogenesis may be related to the location of these enzymes in the pathway and their functions. This also suggests that, in addition to the components that participate in common regulation, there are some special regulatory mechanisms that distinguish their functions and physiological significance.

In summary, through smart-seq2 and PALso-seq2, we found that the absence of *Pan2* does not affect the transcription of mRNA itself, but it seriously interferes with the stability of the poly(A) tail of mRNA. The combined analysis of mass spectrometry and Ribo-lite revealed that this disruption of the tails' stability ultimately leads to abnormal translation during the later stages of spermatogenesis. We further identified PAN2 and its translation-related interacting proteins, such as PABPC1 and EIF4E, through the endogenous IP-MS technique. PAN2 maintains the stability of the poly(A) tail and works in concert with PABPC1 to sustain the translation of long tail mRNA during the transcriptional silencing stage. Taking into account the physiological conditions, the absence of PAN2 leads to the disruption of mRNA tail homeostasis, resulting in the collapse of translation efficiency and the specific stagnation of steps 8–9. These findings describe the stage-specific role of the PAN2–PAN3 complex in male germ cell development and expand the mechanistic framework between poly(A) tail dynamics and translation control and fertility (Fig. 8).

## Methods

### Animals

All mice used in this study were maintained on a C57BL/6J genetic background, and mouse care and experiments were conducted in accordance with the relevant guidelines and regulations of Zhejiang University. The *Pan2*<sup>fl/fl</sup> mouse strain (CKOAI220121QW1) was purchased from Cyagen Biosciences (Suzhou, China). The *Stra8-GFPCre* knock-in mouse line has been reported<sup>52</sup>. *Pan2*<sup>fl/fl</sup> mice were bred with *Stra8-GFPCre* mice to excise *loxP*-flanked exons 7 and 8, thereby generating germ-cell-specific *Pan2*-knockout mice. All experimental procedures were approved by the Zhejiang University Institutional Animal Care and Research Committee (approval #ZJU20250080).

### Cell culture and plasmid transfection

Human embryonic kidney 293T (HEK293T) cells were cultured in Dulbecco's modified Eagle's medium supplemented with 10% fetal bovine serum and 1% penicillin-streptomycin solution. Petri dishes were placed in a humidified incubator at 37 °C in 5% (v/v) CO<sub>2</sub> atmosphere. Transient plasmid transfection of HEK293T cells was performed using Lipofectamine 2000 (Invitrogen, Carlsbad, CA, USA).

### Histological and Immunostaining Analysis

Testis and epididymis samples were fixed in Bouin's solution or 4% paraformaldehyde (158127–500 G; Sigma-Aldrich) overnight,

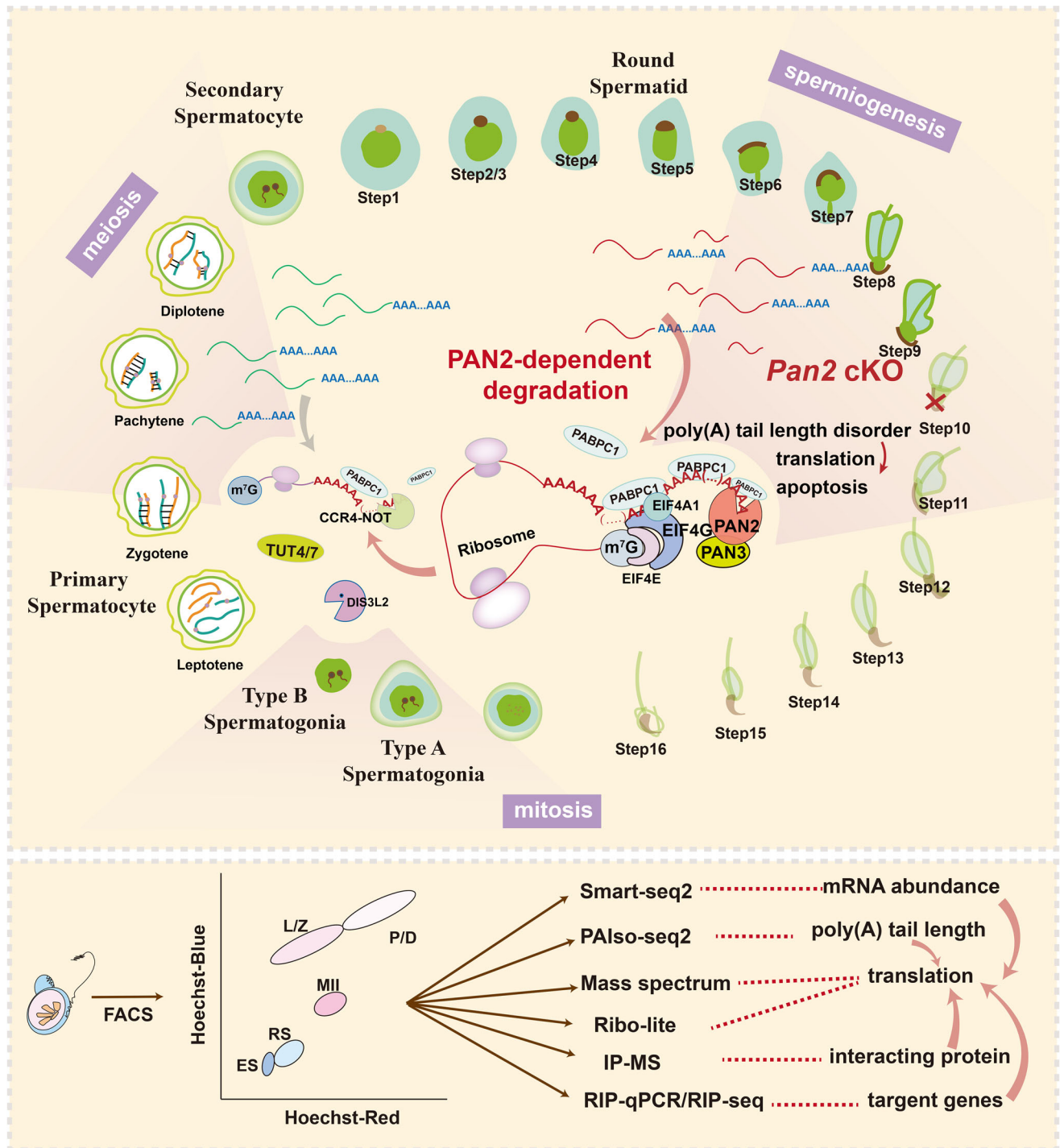


**Fig. 8 | A putative mechanism whereby *Pan2* regulates mRNA poly(A) tail homeostasis and translation during spermiogenesis in mice.** Spermatogenesis is complex and involves a series of steps requiring fine regulation. The process is divided into three main stages: mitosis, meiosis, and spermiogenesis. Different degradation enzymes perform various physiological functions at different stages of spermatogenesis. Our study employed multi-omics combined analysis to reveal the significant role of PAN2 in maintaining the stability of the mRNA poly(A) tail from multiple perspectives such as transcription, poly(A) tail length, and translation. PAN2 is primarily involved in spermiogenesis regulation. It regulates the

deadenylation of mRNAs with long poly(A) tails, maintains overall poly(A) tail homeostasis during spermatogenesis, and ensures normal translation in the later stages. Following the deletion of PAN2, the proportion of long poly(A) tail mRNAs significantly increased. The homeostasis of mRNA poly(A) tails is disrupted, resulting in elongated tails of detailed transcripts and shortened tails of other tailed transcripts. The translation of genes with abnormally elongated or shortened tails is disrupted, leading to a significant decrease in protein expression levels. This process triggers apoptosis and prevented the maturation of round spermatids and causing their premature release from the seminiferous epithelium.

dehydrated in a gradient of ethanol, and sectioned after embedding. For histological analysis, dried sections were deparaffinized, rehydrated, and stained with hematoxylin and eosin (H&E) or periodic acid-Schiff (PAS). Immunohistochemistry was performed according to

standard protocols. For immunofluorescence analyses, after dewaxing and hydration, the sections were boiled in 10 mM sodium citrate buffer (pH 6.0) for 15 min and gradually cooled to room temperature. After washing with phosphate-buffered saline (PBS) with 0.1% Triton X-100

(PBST), the sections were blocked with 5% bovine serum albumin (BSA) for 1 h at room temperature and then incubated with primary antibodies overnight at 4 °C. The next day, the sections were washed three times with PBST and incubated with secondary antibody and 4',6-diamidino-2-phenylindole (Molecular Probes) for 1 h at 25 °C. The samples were then washed, sealed, and imaged using a confocal microscope equipped with a camera.

### Spermatocyte nuclear spreading

The testes were removed from the tunica albuginea, and the seminiferous tubules were exposed to a hypotonic buffer (30 mM Tris, 50 mM sucrose, 17 mM trisodium citrate dihydrate, 5 mM EDTA, 0.5 mM dithiothreitol, and 0.5 mM phenylmethylsulfonyl fluoride; pH 8.2) for 40 min. After the suspension was gently spread onto slides using a 1% paraformaldehyde fixative buffer containing 0.15% Triton X-100 (pH 9.2), the seminiferous tubules were crushed in 100 mM sucrose to disperse single cells and spread onto a thin cell layer on slides. After 2 h of incubation in a humid box at room temperature, the slides were thoroughly air-dried. Immunofluorescence analysis was performed using a standard protocol.

### Metaphase I chromosome spreads

The testes were removed from the tunica albuginea and suspended in isotonic (2.2%) sodium citrate solution. The suspension was centrifuged, resuspended in 1% sodium citrate solution for 15 min, centrifuged again, and fixed in a 3:1 mixture of absolute ethyl alcohol and glacial acetic acid. The fixative was dropped vertically onto previously precooled adhesive slides and dried at room temperature. After washing twice with PBS, the slides were stained with Giemsa stain and sealed.

### Isolation of spermatogenic cells using fluorescence-activated cell sorting

Testes from C57BL/6 mice were collected to prepare spermatogenic cells at different stages using fluorescence-activated cell sorting (FACS). In brief, testicular seminiferous tubules were pretreated with 5 mL of Dulbecco's phosphate-buffered saline (DPBS) (Thermo Fisher Scientific, Waltham, MA, USA; 14190144) containing 120 U/mL collagenase type I (Thermo Fisher Scientific, 17100017) at 32 °C with gentle agitation for 10 min. Dispersed seminiferous tubules were further digested in a reaction mixture containing 5 ml of 0.25% trypsin (Gibco, 25200072) and 0.1 ml of 5 mg/ml DNase I (Sigma-Aldrich, DN25) at 32 °C for 8 min. The digestion was terminated by adding 0.5 ml of fetal bovine serum (FBS) to inactivate trypsin. The resulting cell suspension was filtered through a 70 µm cell strainer (Corning, 352350) DPBS-pre-wetted with DPBS, followed by centrifugation at 500 × g for 5 min at 4 °C. The cell pellet was resuspended in Dulbecco's modified Eagle's medium (DMEM) (Gibco, C11995500BT) to a final concentration of 1 × 10<sup>6</sup> cells/ml, supplemented with Hoechst 33342 (5 µg per 1 × 10<sup>6</sup> cells; Thermo Fisher Scientific). The cell suspension was incubated at 32 °C for 30 min with gentle rotation, then centrifuged at 500 × g for 5 min at 4 °C to discard the supernatant. The collected cells were stained with propidium iodide (1 µg per 1 × 10<sup>6</sup> cells; Sigma-Aldrich, 25535-16-4) at room temperature and subsequently filtered through a 40 µm cell strainer (Corning, 352340). The samples will be subjected to fluorescence-activated cell sorting (FACS) via Hoechst 33342/propidium iodide staining using a flow cytometer (BD Biosciences, FACS Aria II, USA). The instrument will classify cell populations based on fluorescence intensity markers. A 355 nm ultraviolet laser will be used to excite Hoechst 33342 (Thermo Fisher Scientific, H3570), and the dye's broad emission spectrum will be detected through two distinct channels: "Hoechst Blue" (DAPI, 450/20 band-pass filter) and "Hoechst Red" [Indo-1(Blue), 670 LP/610 LP band-pass filter].

### Western blotting

Spermatocytes collected using FACS or lysed using sodium dodecyl sulfate (SDS) sample buffer were heated for 10 min at 95 °C. Lysates were separated through SDS-polyacrylamide gel electrophoresis, electrophoretically transferred to polyvinylidene fluoride membranes (Millipore, Burlington, MA, USA), and blocked with TBST containing 5% (m/v) non-fat milk for 30 min at 25 °C. After probing with primary antibodies, the membranes were washed three times with TBST containing 20 mM Tris-HCl (pH 7.5), 150 mM NaCl, and 0.1% (v/v) Tween-20, and incubated with the corresponding horseradish peroxidase (HRP)-linked secondary antibodies for 1 h at 25 °C. After three washes with TBST, the bound antibodies were detected using WESTAR SUPERNOVA (Cyanagen, Bologna, Italy), according to the manufacturer's instructions. The antibodies and their catalog number and dilutions are presented in Supplementary Table 1.

### RNA sequencing library preparation

Spermatocytes were collected (5000 cells per sample) using FACS. Briefly, each sample with 10 µl of the original volume was lysed using lysis buffer [1% Triton X-100: RNase inhibitor = 4:1, including 0.35 µl of 1:1000 diluted External RNA Controls Consortium (ERCC) spike-in] and incubated with oligo(dT) primer and a deoxynucleoside triphosphate mixture at 72 °C for 3 min, and Smart-seq2 reverse transcription reactions were performed to obtain cDNA. cDNA synthesis was performed using the Smart-seq2 method, as described previously. cDNA (0.5 ng) was used for sequencing library construction using the True-Prep DNA Library Prep Kit V2 for Illumina (Vazyme, Nanjing, China; TD503). Barcoded libraries were pooled and sequenced on the HiSeq X Ten platform (Illumina, San Diego, CA, USA) in the 151 bp paired-end mode.

### RNA sequencing analysis

Raw reads were trimmed and mapped to the mm10 genome. Uniquely mapped reads were employed to quantify gene expression using RSEM software (version 1.3.1). Fragments per kilobase per million mapped reads (FPKM) were calculated to estimate gene expression levels and were normalized to gene length and sequencing depth. The Euclidean distance based on the FPKM values was used to evaluate similarities across biological replicates. Differential gene expression analysis was conducted using the DESeq2 R package. An adjusted  $P < 0.05$  and an absolute fold change  $> 2$  were used as indicators of statistical significance to identify differentially expressed genes (DEGs).

### RNA isolation and quantitative reverse transcription-polymerase chain reaction

Spermatocytes were collected using FACS and lysed directly with 0.2% Triton X-100 and 4 IU of RNase inhibitor. Standard reverse transcription (RT) was performed using random primers and Primer Transcript II Reverse Transcriptase (Takara Bio, Kusatsu, Japan). Real-time polymerase chain reaction (PCR) was performed using Power SYBR Green PCR Master Mix (Applied Biosystems, Life Technologies, Carlsbad, CA, USA) on an Applied Biosystems 7500 Real-Time PCR system. Relative mRNA levels were calculated and compared with the respective (Ct) values normalized to endogenous *GAPDH* mRNA levels. Specifically, the gene expression levels were calculated using  $2^{-\Delta\Delta Ct}$  ( $2^{-\Delta\Delta Ct[\text{gene-Gapdh}]}$ ). The relative transcript levels of the samples were compared with those of the controls, and fold changes were determined. Each experiment was performed in triplicate. The primer sequences are listed in Supplementary Table 2.

### PAIso-seq2

Total RNA was extracted using TRIzol Reagent (Invitrogen, Carlsbad, CA, USA; 15596026), and rRNA was removed using StarPure rRNA depletion pools (Beijing Foreverstar Biotech, Beijing, China; FS-R1051).

Samples were purified using an RNA Clean & Concentrator-5 kit (Zymo Research, Irvine, CA, USA; R1015) coupled with barcode-containing adapters. RNA was reverse transcribed to cDNA, and the second-end PCR handler was added using a unique molecular identifier (UMI)-containing template-switching oligo (TSO). After amplification using 3' adaptor primers and the TSO, the full-length cDNA was concatenated into long molecules for SMRTbell library preparation and sequenced on the PacBio Revio platform (GrandOmics, Beijing, China).

### PAIso-seq2 Data Analysis

The obtained reads were segmented into single PAIso-seq2 cDNA reads using concatenating primers. Segmented reads were split into samples according to their barcodes. Duplicated reads were removed using the UMI sequence, and clean reads were aligned to the mm10 genome (gencode, vM25) using minimaps (v2.24) as described previously<sup>33</sup>. The poly(A) tail information for the clean sequences was extracted and annotated according to a previously published pipeline<sup>54</sup>.

### Poly(A) tail assay

Round spermatid samples ( $10^5$ ) were obtained using FACS, and total RNA was extracted using TRIzol reagent. P1 (GCGAGTCCGCGGCCGCT<sub>12-30</sub>) was anchored to an oligo(dT) using T4 DNA ligase. RT was performed using oligo(dT)-anchored P1 and SuperScript IV (Invitrogen). The samples were then amplified using gene-specific primers (Table S2) and dT-anchored primer P1. The final PCR products were electrophoresed on a 2% agarose gel.

### Endogenous protein immunoprecipitation

Mouse testes from over 8-weeks mice were collected, broken, and lysed with cell lysis buffer (20 mM Tris-HCl, pH 7.5, 80 mM NaCl, 5 mM MgCl<sub>2</sub>, 0.1% Triton-X100, 10% glycerinum, and 20 mM NaF). The lysates were incubated on ice and centrifuged to remove debris, and the resulting supernatants were collected. Specific antibodies and protein A beads (GE Healthcare, Chicago, IL, USA; 10253554) were added to the lysate and incubated at 4 °C for 4 h, then wash beads with cell lysis buffer several times to reduce non-specific interactions. Protein samples were eluted with sodium dodecyl sulfate (SDS) buffer for western blotting or mass spectrometry.

### Ponceau S staining

After the membrane transfer is complete in the Western blot process, take the membrane out from the transfer cassette and rinse it 1–2 times with TBST buffer. Then, completely immerse the membrane in the Ponceau S staining working solution (Sangon Biotech, 6226-75-9) and stain with gentle shaking at room temperature for 5 min, until the protein bands become clearly visible. After staining, take out the membrane and quickly rinse it several times with deionized water. Rinse until the background turns light pink and the protein bands appear red and distinct. At this point, immediately photograph the staining results for documentation. After recording the results, wash the membrane multiple times with TBST until the red color on the membrane completely disappears and the background returns to white. The membrane can then be used for subsequent Western blot steps.

### Co-Immunoprecipitation

The pDEST-HA and pDEST-HA-*Pan2* plasmids were co-transfected with pDEST-Flag-Pabpc1 into HEK293T cells for 48 h. After washing with PBS, the cells were lysed using cell lysis buffer (20 mM Tris-HCl, pH 7.5, 80 mM NaCl, 5 mM MgCl<sub>2</sub>, 0.1% Triton-X100, 10% glycerinum, and 20 mM NaF). The lysates were then rocked at 4 °C for 15 min and centrifuged to get the up-flow part. Approximately 20  $\mu$ L of the supernatant was taken as input, and the remaining fraction was incubated with an EZview™ Red Anti-HA Affinity Gel (Millipore, 308E6779) by rocking at 4 °C for 2–4 h. After washing six times with cell lysis

buffer, the protein samples were eluted with SDS buffer for western blotting.

### RNA pull-down

Testes samples were lysed with Polysome Extraction Buffer (PEB) at 4 °C for 10–20 min. The lysate was then centrifuged at 13,000 rpm for 15 minutes at 4 °C to collect the protein-containing supernatant. An aliquot of this supernatant was combined with an equal volume of 2X SDS loading buffer to prepare the Input sample for later comparison. For the pull-down, an incubation system (500  $\mu$ L total volume) was assembled. It contained approximately 500  $\mu$ g of protein lysate (250  $\mu$ L), 1  $\mu$ L of RNA probes, 250  $\mu$ L of 2X Tris, EDTA, NaCl, Triton Buffer (TENT), 2.5  $\mu$ L of 200X PMSF, 0.5  $\mu$ L of 1000X Aprotinin, 1  $\mu$ L of 400  $\mu$ M VRC, and 2.5  $\mu$ L of 100 U/ $\mu$ L RNase Inhibitor (RRI). The mixture was gently inverted and briefly centrifuged before being incubated with rotation at room temperature for 30 minutes to facilitate RNA-protein binding. Concurrently, streptavidin-coated magnetic beads (50  $\mu$ L) were prepared by washing three times with 500  $\mu$ L of 1X TENT buffer. The washed beads were resuspended in 50  $\mu$ L of 1X TENT and added to the incubation mixture. The combined solution was incubated with rotation either at room temperature for 30 min or at 4 °C for 2 h to capture the RNA-protein complexes onto the beads. After incubation, the beads were separated using a magnetic stand, and the supernatant was discarded. To remove non-specifically bound materials, the beads were washed three times with 500  $\mu$ L of 1X TENT buffer. Bound proteins were eluted by resuspending the beads in 20  $\mu$ L of 1X SDS buffer, followed by heating at 95 °C for 10 min. The eluate was collected after magnetic separation. To maximize yield, the elution step was repeated with another 20  $\mu$ L of 1X SDS buffer. The combined eluates (approximately 40  $\mu$ L) constituted the final pull-down sample for subsequent analysis.

### Low-Input Ribo-Seq

One hundred thousand round spermatids collected with FACS from wild type (WT) and *Pan2*<sup>fl/fl</sup>; *Stra8-Gre* mouse were used for Ribo-lite library construction as previously reported<sup>42</sup>. Briefly, the samples were lysed in lysis buffer (20 mM Tris-HCl, pH 7.4, 150 mM NaCl, 5 mM MgCl<sub>2</sub>, 1 mM DTT, 100  $\mu$ g ml<sup>-1</sup> CHX, 1% Triton X-100; 25 U ml<sup>-1</sup> Turbo DNase (Ambion, AM2239)) for 10 min on ice. The lysates were centrifuged for 10 minutes and treated with RNase I (Ambion, AM2295), and incubated at room temperature for 45 min. After that, SUPERase-In (Ambion, AM2696) was added to terminate the digestion. And then the samples were overlaid by a 700  $\mu$ L sucrose cushion of 1M sucrose in 20 mM Tris-HCl pH 7.4, 150 mM NaCl, 5 mM MgCl<sub>2</sub>, 1 mM DTT, 100  $\mu$ g ml<sup>-1</sup> CHX and 20 U ml<sup>-1</sup> SUPERase-In (Ambion, AM2696) for ultracentrifugation for 4 h at 260,000 g, 4 °C. At the end of ultracentrifugation, the supernatant was discarded and the pellet buffer (10 mM Tris, pH 7.5 and 1% SDS) was used to resuspend the clear round precipitate. RPFs were extracted from pellet buffer with 1 ml TRIzol (Life Technologies, 15596018) and 200  $\mu$ L chloroform. After that, the aqueous phase was precipitated with isopropanol and glycogen. Precipitation was carried out overnight at -20 °C and then by centrifugation at 12,000  $\times$  g, 4 °C for 40 min. RPFs were resuspended in 6  $\mu$ L nuclease-free water and mixed with 6  $\mu$ L gel loading buffer II (Thermo Fisher, AM8546G). The RNA samples were denatured for 90 s at 80 °C, and the RPFs were separated by 15% (wt/vol) polyacrylamide TBE-urea gel for 65 min at 200 V. Extract RNA from the polyacrylamide gel slices by RNA extraction buffer (300 mM sodium acetate, pH 5.5, 1 mM EDTA, and 0.25% SDS). The samples were then frozen at -80 °C for an additional 20 min, thawed at room temperature, and the liquid was transferred to a clean tube. The RNA was extracted using the same procedure described above. The sample underwent sequencing library preparation using the CATS Small RNA-seq Kit (Diagenode, C05010048), which employs a single-tube method involving

polyadenylation, reverse transcription, template switching, and PCR amplification. The DNA library was then purified with AMPure XP (Beckman, A63882). Barcoded libraries were pooled and sequenced on Illumina platforms, generating 150 bp paired-end reads.

### Low-input ribo-seq data analysis

Raw reads were trimmed with cutadapt v1.14 and then mapped to mouse rRNA sequences using Bowtie2 v2.2.2. The remaining fragments after removal of the rRNA from the alignment were aligned to the transcriptome using STAR v2.5.3a. The gene expression levels were calculated using Cufflinks v2.2.1 based on the CDS region annotation from the database of the UCSC genome browser. We then calculated the average FPKM for replicates, considering genes with FPKM > 1 as detected by Ribo-lite<sup>42</sup>.

### Ribonucleoprotein immunoprecipitation assay

Testis lysates were harvested in polysome lysis buffer containing 100 mM KCl; 5 mM MgCl<sub>2</sub>; 10 mM HEPES, pH 7.0; 1% NP40; 1 mM DTT; 1× PMSF; 100 U mL<sup>-1</sup> RRI; and 400 μM VRC. After centrifugation, the supernatant was obtained, and protein A beads (GE Healthcare, 10253554) containing the target endogenous antibody or IgG were added, and the samples were incubated at 4 °C for 4 h. The beads were collected and rinsed eight times with NT2 buffer containing 50 mM Tris-HCl (pH 7.4), 150 mM NaCl, 1 mM MgCl<sub>2</sub>, and 1% NP40. RNA was extracted from the immune complex using an RNA extraction reagent and purified to obtain the target RNA, which was then reverse transcribed into cDNA and analyzed using RT-quantitative polymerase chain reaction (qPCR) or sequencing. The relative abundance of cDNA was analyzed based on the fold change between the ribonucleoprotein immunoprecipitation groups and their corresponding input groups.

### Statistical analysis

Each experiment was repeated at least three times. The results are given as the mean ± standard error of the mean. The results of two experimental groups were compared using a two-tailed unpaired Student's *t*-test. Statistical significance is presented as \**P* < 0.05, \*\**P* < 0.01, \*\*\**P* < 0.001, and \*\*\*\**P* < 0.0001; n.s. indicates *P* > 0.05.

### Reporting summary

Further information on research design is available in the Nature Portfolio Reporting Summary linked to this article.

### Data availability

The smart-seq2 data generated in this study have been deposited in the NCBI Gene Expression Omnibus database under accession number GSE294418. PAIso-seq2 data were deposited in the NCBI Gene Expression Omnibus database under accession number GSE248745. The IP-MS data and Mass spectrometry were deposited in the ProteomeXchange under accession number PXD073956 and PXD064356 [<https://www.iprox.cn/page/home.html>]. The Ribo-lite data and PABPC1 RIP-seq data reported in this paper have been deposited in the Genome Sequence Archive in National Genomics Data Center, China National Center for Bioinformation/Beijing Institute of Genomics, Chinese Academy of Sciences (GSA: CRA033485 and CRA033500), which are publicly accessible at [<https://ngdc.cnbc.ac.cn/gsa>]. Source data are provided with this paper.

### References

- Merrick, W. C. & Pavitt, G. D. Protein synthesis initiation in eukaryotic cells. *Cold Spring Harb. Perspect. Biol.* **10**, a033092 (2018).
- Yi, H. et al. PABP cooperates with the CCR4-NOT complex to promote mRNA deadenylation and block precocious decay. *Mol. Cell* **70**, 1081–1088 e1085 (2018).
- Eisen, T. J. et al. The dynamics of cytoplasmic mRNA metabolism. *Mol. Cell* **77**, 786 (2020).
- Legnini, I., Alles, J., Karaiskos, N., Ayoub, S. & Rajewsky, N. FLAM-seq: full-length mRNA sequencing reveals principles of poly(A) tail length control. *Nat. Methods* **16**, 879 (2019).
- Wolf, J. et al. Structural basis for Pan3 binding to Pan2 and its function in mRNA recruitment and deadenylation. *EMBO J.* **33**, 1514–1526 (2014).
- Schäfer, I. B. et al. Molecular basis for poly(A) RNP architecture and recognition by the Pan2-Pan3 deadenylase. *Cell* **177**, 1619 (2019).
- Dai, X. X. et al. The CNOT4 subunit of the CCR4-NOT complex is involved in mRNA degradation, efficient DNA damage repair, and XY chromosome crossover during male germ cell meiosis. *Adv. Sci.* **8** (2021).
- Berthet, C. et al. CCR4-associated factor CAF1 is an essential factor for spermatogenesis. *Mol. Cell Biol.* **24**, 5808–5820 (2004).
- Nakamura, T. et al. Oligo-astheno-teratozoospermia in mice lacking Cnot7, a regulator of retinoid X receptor beta. *Nat. Genet.* **36**, 528–533 (2004).
- Sha, Q. Q. et al. CNOT6L couples the selective degradation of maternal transcripts to meiotic cell cycle progression in mouse oocyte. *EMBO J.* **37** (2018).
- Morgan, M. et al. A programmed wave of uridylation-primed mRNA degradation is essential for meiotic progression and mammalian spermatogenesis. *Cell Res* **29**, 221–232 (2019).
- Li, N. A. et al. Conditional ablation of DIS3L2 ribonuclease in pre-meiotic germ cells causes defective spermatogenesis and infertility in male mice. *Theranostics* **14**, 5621–5642 (2024).
- Boeck, R. et al. The yeast Pan2 protein is required for poly(A)-binding protein-stimulated poly(A)-nuclease activity. *J. Biol. Chem.* **271**, 432–438 (1996).
- Wilt, F. H. Polyadenylation of maternal rna of sea-urchin eggs after fertilization. *P Natl. Acad. Sci. USA* **70**, 2345–2349 (1973).
- Barkoff, A., Ballantyne, S. & Wickens, M. Meiotic maturation in requires polyadenylation of multiple mRNAs. *EMBO J.* **17**, 3168–3175 (1998).
- Baer, B. W. & Kornberg, R. D. The protein responsible for the repeating structure of cytoplasmic Poly(a)-ribonucleoprotein. *J. Cell Biol.* **96**, 717–721 (1983).
- Subtelny, A. O., Eichhorn, S. W., Chen, G. R., Sive, H. & Bartel, D. P. Poly(A)-tail profiling reveals an embryonic switch in translational control. *Nature* **508**, 66 (2014).
- Lima, S. A. et al. Short poly(A) tails are a conserved feature of highly expressed genes. *Nat. Struct. Mol. Biol.* **24**, 1057 (2017).
- Cheng, S. Y. & Schuh, M. Two mechanisms repress cyclin B1 translation to maintain prophase arrest in mouse oocytes. *Nat. Commun.* **15**, 10044 (2024).
- Borman, A. M., Michel, Y. M. & Kean, K. M. Biochemical characterisation of cap-poly(A) synergy in rabbit reticulocyte lysates: the eIF4G-PABP interaction increases the functional affinity of eIF4E for the capped mRNA 5'-end. *Nucleic Acids Res.* **28**, 4068–4075 (2000).
- Bi, X. P. & Goss, D. J. Wheat germ poly(A)-binding protein increases the ATPase and the RNA helicase activity of translation initiation factors eIF4A, eIF4B, and eIF-iso4F. *J. Biol. Chem.* **275**, 17740–17746 (2000).
- Tarun, S. Z. & Sachs, A. B. Association of the yeast poly(A) tail binding protein with translation initiation factor eIF-4G. *EMBO J.* **15**, 7168–7177 (1996).
- Hess, R. A. & de Franca, L. R. Spermatogenesis and cycle of the seminiferous epithelium. *Adv. Exp. Med. Biol.* **636**, 1–15 (2008).
- Tabar, A. N., Azizi, H., Karoii, D. H. & Skutella, T. Testicular localization and potential function of vimentin-positive cells during spermatogonial differentiation stages. *Animals* **12**, 268 (2022).

25. Kashiwabara, S. I., Nakamshi, T., Kimura, M. & Baba, T. Non-canonical poly(A) polymerase in mammalian gametogenesis. *BBA Regul. Mech.* **1779**, 230–238 (2008).
26. Idler, R. K. & Yan, W. Control of messenger RNA fate by RNA-binding proteins: an emphasis on mammalian spermatogenesis. *J. Androl.* **33**, 309–337 (2012).
27. Kashiwabara, S. et al. Regulation of spermatogenesis by testis-specific, cytoplasmic poly(A) polymerase TPAP. *Science* **298**, 1999–2002 (2002).
28. Hermo, L., Pelletier, R. M., Cyr, D. C. & Smith, C. E. Surfing the wave, cycle, life history, and genes/proteins expressed by testicular germ cells. part 1: background to spermatogenesis, spermatogonia, and spermatocytes. *Microsc. Res. Tech.* **73**, 243–278 (2010).
29. Guo, M. et al. Uncoupling transcription and translation through miRNA-dependent poly(A) length control in haploid male germ cells. *Development* **149**, dev199573 (2022).
30. Czarnocka-Cieciura, A. et al. Comprehensive analysis of poly(A) tails in mouse testes and ovaries using Nanopore Direct RNA Sequencing. *Sci. Data* **12**, 43 (2025).
31. Brouze, M. et al. TENT5-mediated polyadenylation of mRNAs encoding secreted proteins is essential for gametogenesis in mice. *Nat. Commun.* **15**, 5331 (2024).
32. Kleene, K. C., Wang, M. Y., Cutler, M., Hall, C. & Shih, D. Developmental expression of poly(a) binding-protein messenger RNAs during spermatogenesis in the mouse. *Mol. Reprod. Dev.* **39**, 355–364 (1994).
33. Yanagiya, A., Delbes, G., Svitkin, Y. V., Robaire, B. & Sonenberg, N. The poly(A)-binding protein partner Paip2a controls translation during late spermiogenesis in mice. *J. Clin. Investig.* **120**, 3389–3400 (2010).
34. Liu, Y. S., Nie, H., Liu, H. X. & Lu, F. L. Poly(A) inclusive RNA isoform sequencing (PALso-seq) reveals wide-spread non-adenosine residues within RNA poly(A) tails. *Nat. Commun.* **10**, 5292 (2019).
35. Nicholson, A. L. & Pasquinelli, A. E. Tales of detailed Poly(A) Tails. *Trends Cell Biol.* **29**, 191–200 (2019).
36. Liu, Y. S., Nie, H., Zhang, Y. W., Lu, F. L. & Wang, J. Q. Comprehensive analysis of mRNA poly(A) tails by PALso-seq2. *Sci. China Life Sci.* **66**, 187–190 (2023).
37. Chen, Y. et al. Single-cell RNA-seq uncovers dynamic processes and critical regulators in mouse spermatogenesis. *Cell Res* **28**, 879–896 (2018).
38. Margolin, G., Khil, P. P., Kim, J., Bellani, M. A. & Camerini-Otero, R. D. Integrated transcriptome analysis of mouse spermatogenesis. *BMC Genom.* **15**, 39 (2014).
39. Holloway, K. et al. NEK1 facilitates cohesin removal during mammalian spermatogenesis. *Genes* **2**, 260–279 (2011).
40. Rahim, F. et al. A homozygous splicing variant causes asthenozoospermia and flagellar disorganization in a consanguineous family. *Clin. Genet.* **106**, 437–447 (2024).
41. Li, D. F. et al. RNF216 regulates meiosis and PKA stability in the testes. *FASEB J.* **35**, e21460 (2021).
42. Xiong, Z. Q. et al. Ultrasensitive Ribo-seq reveals translational landscapes during mammalian oocyte-to-embryo transition and pre-implantation development. *Nat. Cell Biol.* **24**, 968 (2022).
43. Garneau, N. L., Wilusz, J. & Wilusz, C. J. The highways and byways of mRNA decay. *Nat. Rev. Mol. Cell Bio* **8**, 113–126 (2007).
44. Sassone-Corsi, P. Unique chromatin remodeling and transcriptional regulation in spermatogenesis. *Science* **296**, 2176–2178 (2002).
45. Juliano, C., Wang, J. Q. & Lin, H. F. Uniting germline and stem cells: the function of piwi proteins and the piRNA pathway in diverse organisms. *Annu. Rev. Genet.* **45**, 447–469 (2011).
46. Barckmann, B. et al. Three levels of regulation lead to protamine and Mst77F expression. *Dev. Biol.* **377**, 33–45 (2013).
47. Houben, K. et al. Dynamics and metal exchange properties of C4C4 RING domains from CNOT4 and the p44 subunit of TFIIF. *J. Mol. Biol.* **349**, 621–637 (2005).
48. Dai, P. et al. A translation-activating function of MIWI/piRNA during mouse spermiogenesis. *Cell* **179**, 1566 (2019).
49. Kang, J. Y. et al. LLPS of FXR1 drives spermiogenesis by activating translation of stored mRNAs. *Science* **377**, 727 (2022).
50. Bettegowda, A. & Wilkinson, M. F. Transcription and post-transcriptional regulation of spermatogenesis. *Philos. T R. Soc. B* **365**, 1637–1651 (2010).
51. Braun, R. E. Post-transcriptional control of gene expression during spermatogenesis. *Semin. Cell Dev. Biol.* **9**, 483–489 (1998).
52. Lin, Z. et al. Mettl3/Mettl14-mediated mRNA -methyladenosine modulates murine spermatogenesis. *Cell Res.* **27**, 1216–1230 (2017).
53. Wu, Y. K. et al. ZAR1 and ZAR2 orchestrate the dynamics of maternal mRNA polyadenylation during mouse oocyte development. *Genome Biol.* **26**, 120 (2025).
54. Liu, Y. S., Zhang, Y. W., Wang, J. Q. & Lu, F. L. Transcriptome-wide measurement of poly(A) tail length and composition at sub-nanogram total RNA sensitivity by PALso-seq. *Nat. Protoc.* **17**, 1980–2007 (2022).

## Acknowledgements

We thank the Life Sciences Institute's core facilities at Zhejiang University for their technical assistance. This work was supported by the National Key Research and Development Program of China (2024YFA1803000 to H.-Y.F.), the Guangxi Natural Science Foundation (2024GXNSFAA010083 to L.-L.L.), the National Natural Science Foundation of China (U25A20658, 32170606 to F.-L.L.; 32400703 to L.C.) and the Beijing Natural Science Foundation (7244435 to L.C.). We are grateful to Prof. Ming-Han Tong (CAS Center for Excellence in Molecular Cell Science, Shanghai) for generously sharing the *Stra8-GFPCre* knock-in mouse, and Ying-Ying Huang and Jun-Li Xuan (Core Facilities, School of Medicine, Zhejiang University) for their assistance with cell sorting and confocal FV3000 OSR.

## Author contributions

H.-Y.F. and X.W. conceived the project. H.-Y.F., X.W., L.-L.L., L.C., F.-L.L., and Y.-K.W. designed and analyzed experiments. X.W., Y.-K.W., M.-Y.J., W.-J.W., Z.-Y.J., J.-W.L. and Z.-Y.N. performed experiments. H.-Y.F. and L.C. provided key reagents and materials. X.W. and Y.-K.W. contributed equally to this work. X.W. and H.-Y.F. wrote the paper.

## Competing interests

The authors declare no competing interests.

## Additional information

**Supplementary information** The online version contains supplementary material available at <https://doi.org/10.1038/s41467-026-69639-y>.

**Correspondence** and requests for materials should be addressed to Falong Lu, Lu Chen, Liling Liu or Heng-Yu Fan.

**Peer review information** *Nature Communications* thanks Elizabeth Snyder, and the other, anonymous, reviewer(s) for their contribution to the peer review of this work. A peer review file is available.

**Reprints and permissions information** is available at <http://www.nature.com/reprints>

**Publisher's note** Springer Nature remains neutral with regard to jurisdictional claims in published maps and institutional affiliations.

**Open Access** This article is licensed under a Creative Commons Attribution-NonCommercial-NoDerivatives 4.0 International License, which permits any non-commercial use, sharing, distribution and reproduction in any medium or format, as long as you give appropriate credit to the original author(s) and the source, provide a link to the Creative Commons licence, and indicate if you modified the licensed material. You do not have permission under this licence to share adapted material derived from this article or parts of it. The images or other third party material in this article are included in the article's Creative Commons licence, unless indicated otherwise in a credit line to the material. If material is not included in the article's Creative Commons licence and your intended use is not permitted by statutory regulation or exceeds the permitted use, you will need to obtain permission directly from the copyright holder. To view a copy of this licence, visit <http://creativecommons.org/licenses/by-nc-nd/4.0/>.

© The Author(s) 2026